

THESIS FOR THE DEGREE OF LICENTIATE OF ENGINEERING

Rigid Body Ship Dynamics
System Identification in Calm Waters

MARTIN ALEXANDERSSON



Department of Mechanics and Maritime Sciences
CHALMERS UNIVERSITY OF TECHNOLOGY
Gothenburg, Sweden 2022

Rigid Body Ship Dynamics

System Identification in Calm Waters

MARTIN ALEXANDERSSON

© MARTIN ALEXANDERSSON, 2022

Report No 2022:12

Chalmers University of Technology
Department of Mechanics and Maritime Sciences
SE-412 96, Gothenburg
Sweden
Telephone: +46 (0)31-772 1000
www.chalmers.se

Typeset by the author using L^AT_EX.
Printed by Chalmers Reproservice
Gothenburg, Sweden, 2022

Rigid Body Ship Dynamics

MARTIN ALEXANDERSSON

Chalmers University of Technology

Department of Mechanics and Maritime Sciences

Abstract

It is common today that operational data is recorded onboard ships within the Internet of Ships (IoS) paradigm. This enables the possibility to build ship digital twins as digital copies of the real ships. Predicting the ship's motions with ship dynamics could be an important sub-component of these ship digital twins. A model for the ship's dynamics can be identified based on observations of the ship's motions. The identified model will have model uncertainty due to imperfections and idealizations made in physical model formulations as well as uncertainty from errors in the measurement data, which can be very pronounced when using full scale operational data. It is easier to develop accurate models with low model uncertainty using data obtained in a controlled laboratory environment where the measurement errors are much lower, especially in calm water conditions. The prediction model should be able to describe scenarios that a ship has never encountered before, which is possible if much of the underlying physics has been identified. Grey-box modelling is a technique which combines operational data with physical principles to achieve this.

The objective of this thesis is to develop system identification methods for grey box models with good generalization of the model scale rigid body ship dynamics in calm waters.

A model development procedure is proposed to handle the model uncertainty through the selection of candidate models based on a hold-out evaluation procedure. The measurement noise is handled by an iterative preprocessor, which uses an extended Kalman filter (EKF) and a Rauch Tung Striebel (RTS) smoother that uses an initially estimated predictor model from semi-empirical formulas.

It is demonstrated that the ship's roll motion with high accuracy can be described using a quadratic damping model. For the more complex manoeuvring models, multicollinearity is a large problem where the appropriate complexity needs to be selected with the bias-variance trade-off between underfitting or overfitting the data. Hold-out turning circle tests were predicted with high accuracy for the wPCC and KVLCC2 test case ships with models from the proposed development procedure and parameter estimation method.

The proposed methods can produce prediction models with high generalization given that a suitable model structure has been selected from the candidate models and an appropriate split in the hold-out evaluation of the model development process has been applied.

Keywords: Extended Kalman filter, Inverse dynamics, Multicollinearity, RTS smoother, Ship digital twin, Ship manoeuvring, System identification

Preface

This thesis presents research performed since February 2020 at the Division of Marine Technology, Department of Mechanics and Marine Sciences at Chalmers University of Technology and SSPA Sweden AB (www.sspa.se). Financial support for this research was provided by the DEMOPS project (Development of Methods for Operational Performance of Ships) funded by the Swedish Transport Administration (project: FP4 2020) and the D2E2F project (Data Driven Energy Efficiency of Ships) funded by the Swedish Energy Agency (project: 49301-1).

I had unsuccessfully been applying for funding of my PhD studies for a couple of years when Professor Wengang Mao contacted me three years ago with the offer to become a PhD student. Otherwise, I would probably be still searching for funding. I will always be very grateful for this opportunity. Wengang has also been my main supervisor during my studies, a guide in academic research, and a tutor in statistical and machine learning methods.

This gratitude also goes to my examiner and co-supervisor, Professor Jonas W. Ringsberg, head of the Division of Marine Technology. I have enjoyed our discussions about research methodology and how to organize a paper in academic writing, where his detailed proofreading has also been a great asset.

I also want to thank SSPA Sweden AB for allowing me to be an industrial PhD student within my current employment. A special thanks to Dr. Christian Finnsgård, head of the Research Department at SSPA, for his support and good advice throughout the project. I also want to mention all the personnel at SSPA who have been involved in model tests, building the ship models, and conducting the experiments.

Martin Alexandersson
Göteborg, November 2022

Contents

Abstract	i
Acknowledgments	iii
List of publications	vii
Nomenclature	viii
List of acronyms	xi
1 Introduction	1
1.1 Background	2
1.2 Literature review	3
1.3 Motivation and objective	5
1.4 Assumptions and limitations	6
1.5 Reproducibility	6
1.6 Outline of the thesis	7
2 Rigid body ship dynamics models	9
2.1 Roll motion	9
2.2 Vessel manoeuvring models	10
2.2.1 The propeller model	15
3 Methods	17
3.1 Roll model parameter estimation	17
3.1.1 Derivation approach	17
3.1.2 Integration approach	18
3.2 Manoeuvring model parameter estimation	18
3.2.1 Inverse dynamics and regression	19
3.2.2 Data cleaning	20
3.2.3 Regression	23
3.3 Model development process	24
4 Summary and discussions of appended papers	25
4.1 Summary of Paper 1	25

4.1.1	Best mathematical model for the roll motion	26
4.1.2	Comparison with Ikeda's method	28
4.1.3	Generic roll damping model	30
4.2	Summary of Paper 2	33
4.2.1	The wPCC test case	35
4.2.2	The KVLCC2 test case	40
4.2.3	Inverse dynamics	46
4.2.4	Preprocessing	47
5	Conclusions	49
6	Future work	53
	References	55
A	Initial estimates	61
II	Appended papers	63
1	Analysis of roll damping model scale data	
2	System identification of vessel manoeuvring models	

List of publications

This thesis is based on the following appended papers:

- Paper 1** M. Alexandersson et al. (2021b). “Analysis of roll damping model scale data”. In: *Ships and Offshore Structures* 16.sup1, pp. 85–92. ISSN: 1744-5302. DOI: 10.1080/17445302.2021.1907070.
- Paper 2** M. Alexandersson et al. (2022a). “System identification of vessel manoeuvring models”. en. In: *Ocean Engineering* 266. ISSN: 0029-8018. DOI: 10.1016/j.oceaneng.2022.112940.

Other relevant publications co-authored by Martin Alexandersson:

- Paper** M. Alexandersson et al. (2022b). “A comparison of ship manoeuvrability models to approximate ship navigation trajectories”. In: *Ships and Offshore Structures*. ISSN: 1744-5302. DOI: 10.1080/17445302.2022.2067409.
- Paper** M. Alexandersson et al. (2021a). “Prediction of roll motion using fully nonlinear potential flow and ikeda’s method”. In: *Proceedings of the thirty-first (2021) international ocean and polar engineering conference*. Rhodes, Greece. ISBN: 978-1-880653-82-1.

Nomenclature

β	ship drift angle	rad
∇	ship displacement	m ³
δ	rudder angle	rad
ω_0	natural angular velocity	rad/s
ϕ	ship roll angle	rad
ϕ_a	initial roll amplitude	rad
Ψ	ship heading	rad
ρ	water density	kg/m ³
c	control signal	
w	process noise	
A_0	mid ship area coefficient	
A_{44}	total mass moment of inertia	kg·m ²
B_1	linear damping coefficient	Nm/(rad/s)
B_2	quadratic damping coefficient	Nm/(rad/s ²)
B_3	cubic damping coefficient	Nm/(rad/s) ³
B_{BK}	bilge keel roll damping	Nm/(rad/s)
B_E	eddy roll damping	Nm/(rad/s)
B_F	friction roll damping	Nm/(rad/s)
B_L	hull lift roll damping	Nm/(rad/s)
B_W	wave roll damping	Nm/(rad/s)
<i>beam</i>	ship beam	m
BK_B	bilge keel height	m
BK_L	bilge keel length	m
C_1	linear stiffness coefficient	Nm/rad
C_3	stiffness coefficient	Nm/rad ³
C_5	stiffness coefficient	Nm/rad ⁵
D	propeller diameter	m
g	gravity	kg·m/s ²
GM	ship metacentric height	m
I_z	ship yaw moment of inertia	kg·m ²
J	propeller advance ratio	
L	ship perpendicular length	m
m	ship mass	kg

N	ship yawing moment	Nm
n	propeller speed	rad/s
OG	vertical distance into water from still water to centre of gravity	m
r	yaw rate	rad/s
T	mean draught	m
t	time	s
u	surge velocity	m/s
V	ship speed	m/s
v	sway velocity	m/s
w_p	propeller wake fraction	
w_{p0}	taylor wake fraction	
X	ship force in longitudinal direction	N
x_0	ship global position	m
x_G	ship longitudinal centre of gravity	m
x_p	propeller longitudinal position	m
Y	ship force in transverse direction	N
y_o	ship global position	m

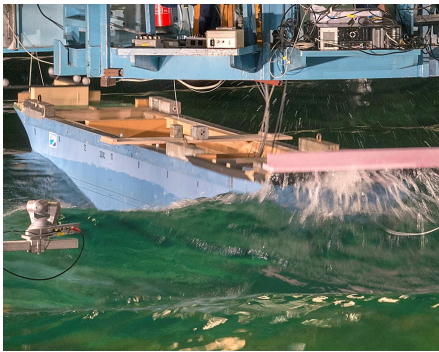
List of acronyms

CFD	–	Computational fluid dynamics
CMT	–	captive model test
DT	–	Digital twin
DOF	–	Degree of freedom
EK	–	Kalman filter
EKF	–	Extended Kalman filter
FFT	–	Fast Fourier transform
HSVA	–	Hamburg ship model basin
IMO	–	International Maritime Organization
IoS	–	Internet of Ships
IoT	–	Internet of Things
MARIN	–	Maritime research institute Netherlands
ML	–	Machine learning
ODE	–	Ordinary differential equation
OLS	–	Ordinary least squares
PMM	–	Planar motion mechanism
RTS	–	Rauch Tung Striebel smoother
SDT	–	Ship digital twin
SI	–	International System of Units
SSPA	–	SSPA Sweden AB (www.sspa.se)
SVR	–	Support vector regression
VCT	–	Virtual captive test
VP	–	Virtual prototyping

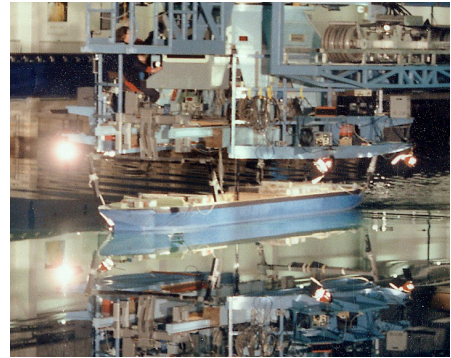
Introduction

The use of twin models is not a new idea. NASA built twin rockets for the Apollo missions, where one rocket went to the Moon and the other twin rocket stayed on Earth. The twin model could have been used as a reference object in case of a mishap during the mission. The twin model concept has many other useful applications, not just for catastrophic scenarios with a failing space ship, but also for more ordinary applications for conventional ships. However, building a real twin ship as a reference object is not realistic. Instead, with data recorded aboard ships, it is possible to build a ship digital twin (SDT) to serve the same purpose. System identification methods of rigid body ship dynamics are presented in this thesis, which can be used to build important sub-components/models in the SDTs.

Ship dynamics is a branch of ship hydrodynamics that concerns the ship's forces and motions when the ship is allowed to move and rotate in all directions. Seakeeping and Manoeuvring are the two major subfields (see Figure 1.1). Seakeeping studies the behavior of a ship in a seaway while it is under the influence of external waves, currents, and wind. Calm water conditions, lacking the external waves, are further assumed in Manoeuvring, which is considered either an idealized and simplified case of Seakeeping or the true conditions in sheltered environments. This chapter first



(a) Seakeeping.



(b) Manoeuvring.

Figure 1.1: Seakeeping and manoeuvring model tests, copyright SSPA.

provides a background by defining the Internet of Ships (IoS), ship digital twins (SDT) and the modelling of rigid body ship dynamics with white-box, black-box, or grey-box models. A literature review of system identification is then presented. The motivation and objective of this research are then stated, followed by the assumptions and limitations.

1.1 Background

With the principles of the Industry 4.0, Shipbuilding 4.0 will transform the design, manufacturing, operation, shipping, services, production systems, maintenance, and value chains in all aspects of the shipbuilding industry (Stanic et al. 2018). The emergence of the Internet-of-Things (IoT) has led to the introduction of the Internet of Ships (IoS) paradigm (Liu et al. 2016).

“IoS is the interconnecting of sensing objects, such as ships, crews, cargoes, onboard equipment, the waterway environment, waterway facilities, shore-based facilities, and other navigation elements. The sensing objects are embedded with various sensor and heterogeneous network technologies that enable them to collect and exchange data.”

Safety enhancements, route planning and optimization, energy efficiency, automatic berthing and autonomous shipping are some of the emerging applications of the IoS (Aslam et al. 2020). A ship digital twin (SDT), which is a digital copy of a real ship, is one way to utilize all data within the IoS (Chen et al. 2021). SDTs are data-driven in contrast to the alternative model-based virtual prototyping (VP) (Major et al. 2021). An SDT is typically used as a model for an existing ship from which data can be collected; the VPs are prototypes for future ships, in which no operational data is available. The models for VP and SDT are categorized as white-box, black-box, or grey-box models. White-box models are used in VP. Either black-box or grey-box models are used in the SDTs.

- White-box modeling
involves applying physical principles to ensure that no observed data is required. One example is computational fluid dynamics (CFD). Semi-empirical models, in which unknown physical constants have been derived from historical experiments, could also be considered white-box models (Leifsson et al. 2008).
- Black-box modeling
means that parameters do not have physical significance and that the objective is to find an effective model that fits the observed data (Lindskog and Ljung 1995).
- Grey-box modeling
is using a combination of white-box and black-box modeling methods to ensure that both a physical model and data are used. This concept is also referred to as semi-physical modeling, hybrid modeling, or semi-mechanistic modeling in the literature (Leifsson et al. 2008).

The white and black component can be combined as a grey box model in several ways, using either a serial or parallel approach (Leifsson et al. 2008) as seen in Figure 1.2.

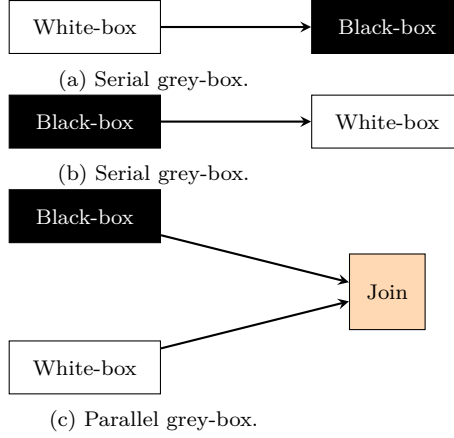


Figure 1.2: Several ways to combine white- and black-box models in grey box models.

1.2 Literature review

Ship digital twin (SDT) has a positive trend in the number of publications in recent years (2018-2021). Most of the papers concern ship equipment such as electric power systems, propulsion system, ship hull structure, and marine diesel engines. A small minority of the SDT applications handle ship trajectory, speed, and fuel consumption (Assani et al. 2022). Even though SDT is not explicitly mentioned, there are many publications about methods that can be used as SDTs. Lang et al. (2022) predicted the propulsion power for a chemical tanker for three test case voyages by using ML black-box modeling. However, the manoeuvres were excluded. Nielsen et al. (2022) used grey-box modelling for the manoeuvring prediction of a ferry, where a deep learning model (black-box) captures the residues between a first-principles model (white-box) and observed data. These studies demonstrate the vast potential within the field.

Noteworthy publications within the system identification of the ship's manoeuvring dynamics are summarized in Table 1.1 and categorized as black-box or grey-box models. The system identification can be applied to full scale data (Åström and Källström 1976; Revestido Herrero and Velasco González 2012; Perera et al. 2015), which has the highest model uncertainty and measurement uncertainty. Therefore, it is the hardest task but also the most relevant. A method for reducing the uncertainty is using model test data (Araki et al. 2012; Luo et al. 2016; Xue et al. 2021; Miller 2021; He et al. 2022). The uncertainty can be further reduced by using simulated data (Shi et al. 2009; Zhu et al. 2017; Wang et al. 2021), which can demonstrate the potential of new methods that have the benefit of the true model being known. One must however be consistent with the main objective of identifying real objects, not only mathematical models (Miller 2021).

Black-box modeling was used in He et al. (2022), using a neural network, and in

Table 1.1: System identification references, black-box (BB), grey-box (GB).

Method	BB	GB	Data	Reference
Genetic algorithm	✓		Lake test	Miller (2021)
Neural network	✓		Model test	He et al. (2022)
Gaussian process	✓		Model test	Xue et al. (2021)
Kalman filter maximum likelihood		✓	Full scale	Åström and Källström (1976)
Unscented Kalman filter		✓	Full scale	Revestido Herrero and Velasco González (2012)
Extended Kalman filter		✓	Full scale	Perera et al. (2015)
Extended Kalman filter		✓	Simulated	Shi et al. (2009)
Constrained least squares		✓	Model test, CFD	Araki et al. (2012)
Support vector regression		✓	Simulated	Zhu et al. (2017), Wang et al. (2021)
Support vector regression		✓	Model test	Luo et al. (2016)

Xue et al. (2021), using a Gaussian process. The nonparametric models are related because the system structure is known but no parameters are required; this is seen in Pongduang et al. (2020). However, most of the system identification methods for ship manoeuvring models use grey-box modeling by assuming a predefined mathematical model, which reduces the problem to a parameter estimation. The Kalman filter (KF) combined with maximum likelihood estimation was proposed in 1976 by Åström and Källström (1976) to develop a linear manoeuvring model that utilized manually recorded data in 1969 aboard the Atlantic Song freighter. The extended Kalman filter (EKF) can also estimate parameters if the parameters are represented as states of the state space model. This technique was used on a nonlinear Nomoto model (Perera et al. 2015) and a 3 degree of freedom model (3DOF) (Shi et al. 2009). The EKF was used in Araki et al. (2012), with constrained parameters based on physical reasoning and prior knowledge from constrained least squares regression. The unscented Kalman filter (UKF), which has been proposed as an improvement to the EKF for handling nonlinear systems, was used in Revestido Herrero and Velasco González (2012). Support vector regression (SVR) has also been investigated by Luo et al. (2016), Zhu et al. (2017), and Wang et al. (2021). A genetic algorithm was used by Miller (2021) for the system identification of a model test performed on a lake.

1.3 Motivation and objective

A profuse amount of data concerning the operation of ships in the oceans is collected daily. Many uses and potential applications of this data remains to be discovered. The use of SDTs (which are modelled as white-boxes, black-boxes, or grey-boxes) has potential. Black-box modeling is entirely data-driven, which means that no prior understanding of the system generating the data is needed. Therefore, it is an attractive option for the SDT modelling. One caveat is that the black-box modeling may provide infeasible models outside of the domain covered by the available data (Nielsen et al. 2022).

The white-box modeling, which is not relying on the data, does not have this problem. However, to obtain high accuracy it does require a complete understanding of the system. Acquiring such knowledge may be possible for some cases with CFD calculations, but it is not practical for the complex environment and nonlinearities of a ship operating at sea (Miller 2021). Wind, waves, and currents add uncertainty to the modelling in the deep sea. Water depth and the bank effect add uncertainty in coastal areas (Nielsen et al. 2022). Even if the sea is flawlessly modelled, long-term predictions with high accuracy will be exposed to deterministic chaos (Lorenz 1963), which is popularly known as the butterfly effect. During the butterfly effect, only a very small difference in the initial conditions results in a significantly different outcome. For instance, a period of two weeks is believed to be the upper limit for weather forecasts (Zhang et al. 2019). Because the methods developed in this thesis frame the first step towards system identification in full scale sea conditions, grey-box modelling is used. The grey-box model involves merging the white-box and black-box methods in an attempt to alleviate concerns regarding both models.

It is practical to first assume higher levels of simplifications and approximations for the problem under study and thereafter increase the complexity of the problem step by step. The effects of various factors can be initially studied in isolation with this approach. rigid body ship dynamics at full scale sea conditions comprises uncertainties from:

- the **environment**: wind, waves, and currents
- the **ship**: geometry and mass properties
- the **measurements**

The simplification this thesis presents is limiting the uncertainties at full scale sea conditions by using model test data from a controlled laboratory environment. The main objective of this thesis is to:

develop system identification methods for grey box models with good generalization of the model scale rigid body ship dynamics in calm waters.

To fulfill the research objective, the goals for this thesis have been formulated by following the step-by-step approach. The approach consists of reducing complexity and then gradually increasing the model complexity:

Roll motion model

The first goal of the thesis is to develop a model for the calm water rigid body ship dynamics in the roll degree of freedom; it is based on model test data.

Manoeuvring model

The second goal is to increase the complexity and uncertainty of the modelling by adding the surge, sway, and yaw degrees of freedom, which addresses the manoeuvring problem.

Model generalization

The third goal is a constraint. In order to be of practical use in the internet of ships (IoS) applications, the models must be able to make predictions outside of the domain covered by the available data.

1.4 Assumptions and limitations

The calm water condition is used as a simplification of the real sea condition that a ship encounters. This condition does not account for the factors of wind, waves, and currents. These assumptions simplify the system identification by reducing the degrees of freedom to: surge, sway, yaw and, roll. The rigid body assumption simplifies the ship to a stiff body that does not transform under the influence of forces. It is important to note that all results are not necessarily directly transferable to the full scale when model scale data is used considering potential scale effects.

1.5 Reproducibility

The research for this thesis has been conducted with the aim of having a high degree of reproducibility. The U.S. National Science Foundation (NSF) subcommittee on replicability in science defines reproducibility as (Bollen et al. 2015):

“Reproducibility refers to the ability of a researcher to duplicate the results of a prior study using the same materials and procedures as were used by the original investigator. ... Reproducibility is a minimum necessary condition for a finding to be believable and informative.”

To ensure adequate reproducibility, all code developed in this research has been made available as open source. In addition, the used data has been published as open data, as seen in the references in Table 1.2. Publishing the roll decay data from Paper 1 as open data was not possible due to intellectual property (IP) rights.

Table 1.2: References for reproducibility.

Paper	Code	Data
1	Alexandersson (2022b)	Unpublished due to IP rights
2	Alexandersson (2022a)	Alexandersson (2022c), Stern et al. (2011)

1.6 Outline of the thesis

Chapter 2 presents the models for rigid body ship dynamics used in this thesis. The models for roll motion are introduced in section 2.1, and the manoeuvring motion models are introduced in section 2.2. These models represent the physical principles and thereby the white-box component of the developed grey-box models. Parameter estimations, representing the black-box component, are used to regress the parameters of the white-box models. The parameter estimations are introduced in chapter 3 for the roll motion and the manoeuvring motion in section 3.1 and section 3.2. A summary of the appended papers, which includes research activities and a selection of the most relevant results, is presented in chapter 4, followed by the conclusions in chapter 5 and plans for future work in chapter 6.

Rigid body ship dynamics models

The dynamics of a ship comprise a variety of forces and motions in the six degrees of freedom (6DOF): surge, sway, heave, roll, pitch, and yaw. Heave and pitch motions are neglected in calm water conditions to ensure that a four degrees of freedom (4DOF) model can sufficiently express the ship's dynamics. Models for roll and the manoeuvring model for the remaining DOFs are presented in section 2.1 and section 2.2.

2.1 Roll motion

The roll motion without manoeuvres or external forces can be expressed by (Himeno 1981),

$$A_{44}\ddot{\phi} + B_{44}(\dot{\phi}) + C_{44}(\phi) = 0 \quad (2.1)$$

where the static stability of the ship is expressed as the stiffness $C_{44}(\phi)$ with a function of the roll angle ϕ , the damping $B_{44}(\dot{\phi})$ with a function of the roll velocity $\dot{\phi}$ and inertia A_{44} connected to the roll acceleration $\ddot{\phi}$. The ship's roll motion can be observed under these conditions in a roll-decay test. The model is forced to an initial roll angle, as seen in Figure 2.1a. The model is then released (Figure 2.1b) and rolls back to equilibrium (Figure 2.1c). The model will pass this static equilibrium point as a result of momentum and not stop until it has reached the end point on the other side (Figure 2.1d). This motion starts a new cycle in which the model rolls back again. This new cycle results in oscillatory motion where potential energy is transferred to kinetic energy and back to potential energy.

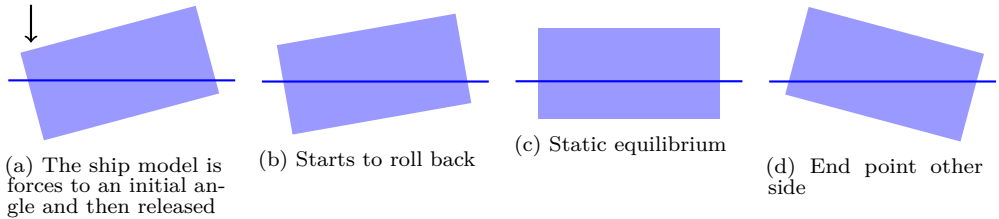


Figure 2.1: Roll decay test.

This oscillation would never end if it was not for the roll damping. Interactions between the ship and the water, such as friction, wave generation, eddy generation, and hydrodynamic lift, will cause the ship to lose some of its energy. The energy loss means that the oscillation is decaying over time, as seen in Figure 2.2, which displays the time series for the roll angle.

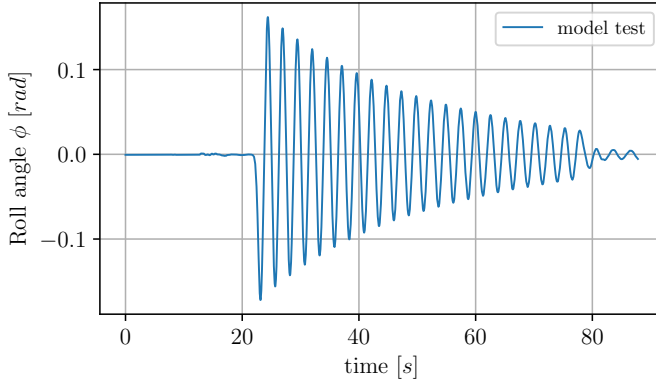


Figure 2.2: Example roll decay signal.

The damping $B_{44}(\dot{\phi})$ can be expressed as an expansion series:

$$B_{44}(\dot{\phi}) = B_1 \cdot \dot{\phi} + B_2 \cdot \dot{\phi} |\dot{\phi}| + B_3 \cdot \dot{\phi}^3 + \dots + B_n \cdot \dot{\phi}^n \quad (2.2)$$

This series can be truncated to be expressed as a “linear model” (Eq. (2.3)), “quadratic model” (Eq. (2.4)), and “cubic model” (Eq. (2.5)).

$$A_{44}\ddot{\phi} + B_1\dot{\phi} + C_1\phi = 0 \quad (2.3)$$

$$A_{44}\ddot{\phi} + C_1\phi + (B_1 + B_2 |\dot{\phi}|) \dot{\phi} = 0 \quad (2.4)$$

$$A_{44}\ddot{\phi} + (B_1 + B_2 |\dot{\phi}| + B_3 \dot{\phi}^2) \dot{\phi} + (C_1 + C_3 \phi^2 + C_5 \phi^4) \phi = 0 \quad (2.5)$$

Models for the remaining degrees of freedom are presented in the next section.

2.2 Vessel manoeuvring models

Ship manoeuvring is a simplified case of seakeeping. The encountering waves have been removed, assuming calm water conditions. The manoeuvring motions have low frequencies so that added masses and other hydrodynamic derivatives can be assumed as constants (Fossen 2021). Three manoeuvring models are used in this thesis:

- Linear (LVMM) (Matusiak 2021)
- Abkowitz (AVMM) (Abkowitz 1964)
- Modified Abkowitz (MAVMM), which is proposed in Paper 2

Figure 2.3 shows the reference frames used in the manoeuvring models where x_0 and y_0 and heading Ψ are the global position and orientation of a ship fix reference frame $O(x, y, z)$ (or rather $O(x, y)$ when heave is excluded) with origin at midship. u, v, r, X, Y and N are velocities and forces in the ship fix reference frame.

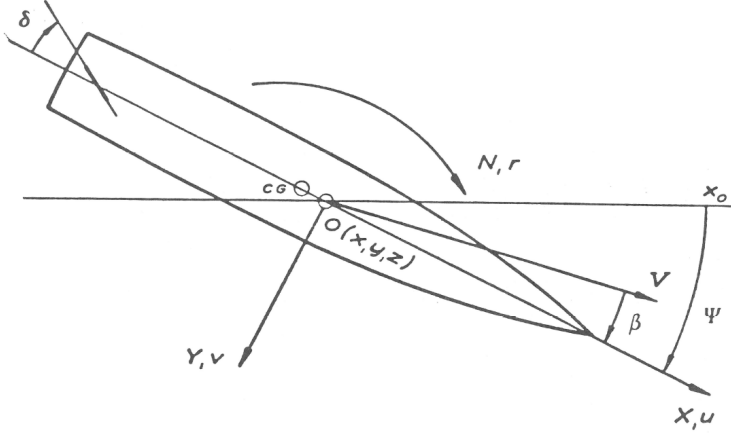


Figure 2.3: Reference frames.

The manoeuvring equation can be described as (Fossen 2021),

$$\begin{bmatrix} -X_{\dot{u}} + m & 0 & 0 \\ 0 & -Y_{\dot{v}} + m & -Y_{\dot{r}} + mx_G \\ 0 & -N_{\dot{v}} + mx_G & I_z - N_{\dot{r}} \end{bmatrix} \begin{bmatrix} \dot{u} \\ \dot{v} \\ \dot{r} \end{bmatrix} = \begin{bmatrix} mr^2 x_G + mrv + X_D(u, v, r, \delta, thrust) \\ -mru + Y_D(u, v, r, \delta, thrust) \\ -mru x_G + N_D(u, v, r, \delta, thrust) \end{bmatrix} \quad (2.6)$$

where the first matrix describes the inertia of the ship in the surge, sway and yaw directions. The inertia in air is represented by the mass m and moment of inertia I_z . The added mass in water is represented by: $X_{\dot{u}}$, $Y_{\dot{v}}$, $Y_{\dot{r}}$, $N_{\dot{v}}$ and $N_{\dot{r}}$. The hydrodynamic forces from the ship hull and rudder are described in the functions $X_D()$, $Y_D()$ and $N_D()$. The accelerations (\dot{u} , \dot{v} and \dot{r}) can be solved from this equation,

$$\dot{\nu} = \begin{bmatrix} \dot{u} \\ \dot{v} \\ \dot{r} \end{bmatrix} = \begin{bmatrix} \frac{1}{-X_{\dot{u}} + m} & 0 & 0 \\ 0 & -\frac{I_z + N_{\dot{r}}}{S} & -\frac{-Y_{\dot{r}} + mx_G}{S} \\ 0 & -\frac{-N_{\dot{v}} + mx_G}{S} & -\frac{Y_{\dot{v}} - m}{S} \end{bmatrix} \begin{bmatrix} mr^2 x_G + mrv + X_D(u, v, r, \delta, thrust) \\ -mru + Y_D(u, v, r, \delta, thrust) \\ -mru x_G + N_D(u, v, r, \delta, thrust) \end{bmatrix} \quad (2.7)$$

where S is a helper variable:

$$S = -I_z Y_{\dot{v}} + I_z m + N_{\dot{r}} Y_{\dot{v}} - N_{\dot{r}} m - N_{\dot{v}} Y_{\dot{r}} + N_{\dot{v}} m x_G + Y_{\dot{r}} m x_G - m^2 x_G^2 \quad (2.8)$$

A state space model for manoeuvring can now be defined with six states:

$$\mathbf{x} = \begin{bmatrix} x_0 \\ y_0 \\ \Psi \\ u \\ v \\ r \end{bmatrix} \quad (2.9)$$

where x_0 , y_0 and Ψ are the global coordinates and heading of the ship and u , v and r are the velocities as seen in Figure 2.3. The time derivative of this state $\dot{\mathbf{x}}$ can be defined by a state transition $f(\mathbf{x}, \mathbf{c})$ using geometrical relations how global coordinates x_0 , y_0 and Ψ depend on u , v , and r viz.,

$$\dot{\mathbf{x}} = f(\mathbf{x}, \mathbf{c}) + \mathbf{w} = \begin{bmatrix} \dot{x}_0 \\ \dot{y}_0 \\ \dot{\Psi} \\ \dot{u} \\ \dot{v} \\ \dot{r} \end{bmatrix} + \mathbf{w} = \begin{bmatrix} u \cos(\Psi) - v \sin(\Psi) \\ u \sin(\Psi) + v \cos(\Psi) \\ r \\ \dot{u} \\ \dot{v} \\ \dot{r} \end{bmatrix} + \mathbf{w} \quad (2.10)$$

where \mathbf{c} is control inputs (rudder angle δ and thrust); the last three derivatives: \dot{u} , \dot{v} , \dot{r} are calculated with Eq. (2.7). \mathbf{w} is the process noise, i.e., the difference between the predicted state by the manoeuvring model and the true state of the system. \mathbf{w} is unknown when the manoeuvring model is used for manoeuvre predictions and therefore normally assumed to be zero, but it is an important factor when the manoeuvring model is used in the EKF (see subsection 3.2.2). The manoeuvring simulation can now be conducted by numerical integration of Eq. (2.10). The main difference between the manoeuvring models lies in how the hydrodynamic functions $X_D(u, v, r, \delta, thrust)$, $Y_D(u, v, r, \delta, thrust)$, $N_D(u, v, r, \delta, thrust)$ are defined. These expressions are denoted in prime system (X'_D , Y'_D , N'_D) below for the various manoeuvring models: LVMM, AVMM and MAVMM.

Linear vessel manoeuvring model (LVMM) (Matusiak 2021)

$$X'_D(u', v', r', \delta) = X_\delta \delta + X_r r' + X_u u' + X_v v' \quad (2.11)$$

$$Y'_D(u', v', r', \delta) = Y_\delta \delta + Y_r r' + Y_u u' + Y_v v' \quad (2.12)$$

$$N'_D(u', v', r', \delta) = N_\delta \delta + N_r r' + N_u u' + N_v v' \quad (2.13)$$

Abkowitz vessel manoeuvring model (AVMM) (Abkowitz 1964)

$$\begin{aligned} X'_D(u', v', r', \delta, thrust') = & X_{\delta\delta} \delta^2 + X_{r\delta} \delta r' + X_{rr} r'^2 + X_T thrust' + X_{u\delta\delta} \delta^2 u' \\ & + X_{ur\delta} \delta r' u' + X_{urr} r'^2 u' + X_{uuu} u'^3 + X_{uu} u'^2 \\ & + X_{uv\delta} \delta u' v' + X_{uvr} r' u' v' + X_{uvv} u' v'^2 \\ & + X_u u' + X_{v\delta} \delta v' + X_{vr} r' v' + X_{vv} v'^2 \end{aligned} \quad (2.14)$$

$$\begin{aligned}
 Y_D'(u', v', r', \delta, thrust') = & Y_{0uu}u'^2 + Y_{0u}u' + Y_0 + Y_{\delta\delta\delta}\delta^3 + Y_{\delta\delta}\delta + Y_{r\delta\delta}\delta^2r' + Y_{rr\delta}\delta r'^2 \\
 & + Y_{rrr}r'^3 + Y_r r' + Y_{T\delta}\delta thrust' + Y_T thrust' + Y_{u\delta}\delta u' \\
 & + Y_{ur}r'u' + Y_{uu\delta}\delta u'^2 + Y_{uur}r'u'^2 + Y_{uvv}u'^2v' + Y_{uv}u'v' \\
 & + Y_{v\delta\delta}\delta^2v' + Y_{vr\delta}\delta r'v' + Y_{vrr}r'^2v' + Y_{vv\delta}\delta v'^2 + Y_{vvr}r'v'^2 \\
 & + Y_{vvv}v'^3 + Y_v v'
 \end{aligned} \tag{2.15}$$

$$\begin{aligned}
 N_D'(u', v', r', \delta, thrust') = & N_{0uu}u'^2 + N_{0u}u' + N_0 + N_{\delta\delta\delta}\delta^3 + N_{\delta\delta}\delta + N_{r\delta\delta}\delta^2r' + N_{rr\delta}\delta r'^2 \\
 & + N_{rrr}r'^3 + N_r r' + N_{T\delta}\delta thrust' + N_T thrust' + N_{u\delta}\delta u' \\
 & + N_{ur}r'u' + N_{uu\delta}\delta u'^2 + N_{uur}r'u'^2 + N_{uvv}u'^2v' + N_{uv}u'v' \\
 & + N_{v\delta\delta}\delta^2v' + N_{vr\delta}\delta r'v' + N_{vrr}r'^2v' + N_{vv\delta}\delta v'^2 + N_{vvr}r'v'^2 \\
 & + N_{vvv}v'^3 + N_v v'
 \end{aligned} \tag{2.16}$$

Modified Abkowitz vessel manoeuvring model (MAVMM)

Only the most relevant coefficients in AVMM are included, as proposed in Paper 2.

$$X_D'(u', v', r', \delta, thrust') = X_{\delta\delta}\delta^2 + X_{rr}r'^2 + X_T thrust' + X_{uu}u'^2 + X_u u' + X_{vr}r'v' \tag{2.17}$$

$$\begin{aligned}
 Y_D'(u', v', r', \delta, thrust') = & Y_{\delta\delta}\delta + Y_r r' + Y_{T\delta}\delta thrust' + Y_T thrust' + Y_{ur}r'u' + Y_u u' \\
 & + Y_{vv\delta}\delta v'^2 + Y_v v'
 \end{aligned} \tag{2.18}$$

$$\begin{aligned}
 N_D'(u', v', r', \delta, thrust') = & N_{\delta\delta}\delta + N_r r' + N_{T\delta}\delta thrust' + N_T thrust' + N_{ur}r'u' + N_u u' \\
 & + N_{vv\delta}\delta v'^2 + N_v v'
 \end{aligned} \tag{2.19}$$

The hydrodynamic functions above are expressed using nondimensional units with the prime system, denoted by the prime symbol ($'$). The quantities are expressed in the prime system, using the denominators in Table 2.1. For instance, surge linear velocity u can be expressed in the prime system as seen in Eq. (2.20) using the linear velocity denominator.

$$u' = \frac{u}{V} \tag{2.20}$$

Equations can either be written in the Prime or regular Standard Institute (SI) system. The hydrodynamic derivatives are always expressing forces in the prime system as

Table 2.1: Prime system denominators.

Quantity	Denominators
angle	1
angular acceleration	$\frac{V^2}{L^2}$
angular velocity	$\frac{V}{L}$
area	L^2
density	$\frac{\rho}{2}$
force	$\frac{L^2 V^2 \rho}{2}$
frequency	$\frac{V}{L}$
inertia moment	$\frac{L^5 \rho}{2}$
length	L
linear acceleration	$\frac{V^2}{L}$
linear velocity	V
mass	$\frac{L^3 \rho}{2}$
moment	$\frac{L^3 V^2 \rho}{2}$
time	$\frac{L}{V}$
volume	L^3

function of state variables. The (') sign is therefore implicit and not written out as seen in Eq. (2.21).

$$Y'_{\delta'} = \frac{\partial Y'_D}{\partial \delta'} := Y_{\delta} \quad (2.21)$$

The exceptions are the added masses ($X_{\ddot{u}}$, $Y_{\ddot{v}}$, $Y_{\ddot{r}}$, $N_{\ddot{v}}$ and $N_{\ddot{r}}$) which are expressed in both Prime system or the regular SI system where the (') sign is therefore explicitly stated. There is however a great benefit in expressing the hydrodynamic forces in the prime system. The forces are often nonlinear due to a quadratic relation to the flow velocity, as seen in Eq. (2.22).

$$Y_D = Y_{\delta} \cdot \delta \cdot \frac{L^2 V^2 \rho}{2} \quad (2.22)$$

which becomes linear when expressed in the prime system as seen in Eq. (2.23).

$$Y'_D = Y_{\delta} \cdot \delta' \quad (2.23)$$

2.2.1 The propeller model

A propeller model is developed based on Manoeuvring Modeling Group (MMG) model (Yasukawa and Yoshimura 2015) where the thrust is expressed as:

$$thrust = D^4 K_T n^2 \rho \quad (2.24)$$

and the thrust coefficient K_T is modelled as a second order polynomial:

$$K_T = J^2 k_2 + J k_1 + k_0 \quad (2.25)$$

The advance ratio J is calculated as:

$$J = \frac{u(1 - w_p)}{Dn} \quad (2.26)$$

where D is propeller diameter, n is propeller speed and w_p is the wake fraction at an oblique inflow to the propeller from the drift angle and the yaw rate. A semi-empirical formula for w_p is provided in the MMG model. As an alternative, a simple polynomial is proposed in Eq. (2.27).

$$w_p = C_1 \delta + C_2 \delta^2 + C_3 \beta_p^2 + C_4 u + w_{p0} \quad (2.27)$$

w_p is modeled as a function of rudder angle δ , to include wake influence from the rudder and ship speed u , to include a speed dependency. The influence from drift angle β and yaw rate r is expressed by β_p in Eq. (2.28).

$$\beta_p = \beta - \frac{r}{V} \cdot x_p \quad (2.28)$$

where x_p is the propeller longitudinal position and w_{p0} is the regular Taylor wake fraction, applicable to straight ahead steaming with no rudder angle. Similar to the MMG propeller model, two sets of parameters C_1 - C_4 should be used in the propeller model depending on the sign of β_p .

Methods

The system identification of rigid body ship dynamics can be simplified into parameter estimation if parameterized physical models is assumed as the most appropriate model from a collection of candidate models. The parameter estimations for roll motion and manoeuvring are presented in section 3.1 and section 3.2. The most appropriate models are selected in the model development process which is described in section 3.3.

3.1 Roll model parameter estimation

Parameter estimation can be applied to identify the roll damping parameters (B_1 , B_2 , B_3) and stiffness parameters (C_1 , C_3 , C_5) in the parameterized roll motion models from the previous chapter (Eq. (2.3), Eq. (2.4) and Eq. (2.5)). These equations do not have unique solutions because each equation can be multiplied by an arbitrary factor to obtain a new valid solution. Inertia is therefore excluded to obtain unique solutions. This is achieved by normalizing the equations by the total roll inertia A_{44} , as seen in Eq. (3.1), for the linear model.

$$\ddot{\phi} + \frac{B_1}{A_{44}}\dot{\phi} + \frac{C_1}{A_{44}}\phi = \ddot{\phi} + B_{1A}\dot{\phi} + C_{1A}\phi = 0 \quad (3.1)$$

The identified normalized damping and stiffness parameters B_{1A} and C_{1A} can be expressed in dimensional units by multiplication with the normalization factor A_{44} . If A_{44} is unknown before hand, it can be calculated using Eq. (3.2) (Piehl 2016), assuming that the meta center height GM is known.

$$A_{44} = \frac{GMgm}{\omega_0^2} \quad (3.2)$$

The frequency ω_0 can be obtained with Fast Fourier transform (FFT) of the roll signal. Two methods for parameter estimation have been investigated: the “derivation approach”, referred to in IMO (2006), and the “integration approach” used in Söder et al. (2019b) which are both described in the next subsections.

3.1.1 Derivation approach

In the derivation approach, Eq. (3.1) is treated as a linear regression problem, where the states (ϕ , $\dot{\phi}$, $\ddot{\phi}$) are known and the parameters B_1 and C_1 must be regressed. Only roll angle ϕ is known from the experimental data, which means that the velocity and acceleration $\dot{\phi}$, $\ddot{\phi}$ also must be estimated (note that this is done with numerical differentiation in Paper 1 and with the extended Kalman filter (EKF) in Paper 2). A least squares fit must be applied to the roll motion equation to identify the damping and stiffness parameters.

3.1.2 Integration approach

In the integration approach, Eq. (3.1) is solved as an ordinary differential equation (ODE) for many estimated sets of parameters until the solution converges. This method is time-consuming, and convergence is not guaranteed. However, the advantage is that only roll angle ϕ is needed.

3.2 Manoeuvring model parameter estimation

A new parameter estimation method is proposed in Paper 2 for the remaining degrees of freedom. A manoeuvring model is used to solve the reversed manoeuvring problem. The problem may consist of predicting unknown forces from known manoeuvring model test data. The hydrodynamic derivatives in the manoeuvring model can be identified through regression of the force polynomials on forces predicted with inverse dynamics (see subsection 3.2.1). The measurement noise must be removed prior to the regression of hydrodynamic derivatives in the manoeuvring model. This is conducted by an extended Kalman filter (EKF) and a Rauch Tung Striebel (RTS) smoother (see subsection 3.2.2). The EKF requires an accurate manoeuvring model as the predictor. Therefore, the accurate manoeuvring model is both the input and output of the method. As a solution to this dilemma, a linear manoeuvring model that includes hydrodynamic derivatives estimated with semi-empirical formulas (Appendix A) is used as the initial predictor. Once the regressed manoeuvring model has been obtained, the parameter estimation can be refined, using the regressed manoeuvring model as the predictor model in the EKF, to improve the filter and obtain a more accurate manoeuvring model. The method is summarized in Figure 3.1 and can be repeated several times (indicated by the dashed arrow) for improved accuracy.

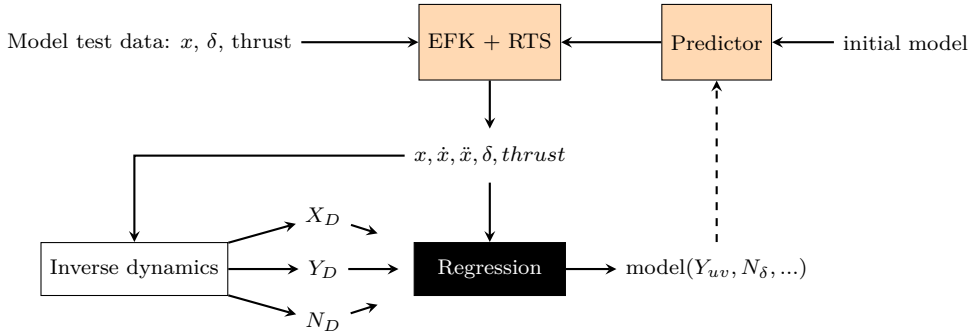


Figure 3.1: Method to estimate the manoeuvring model hydrodynamic derivatives.

Using semi-empirical formulas (Appendix A) for the initially estimated manoeuvring model adds prior knowledge about the ship dynamics to the regression. An example, with simulation results from the steps in the iteration, is presented in Figure 3.2.

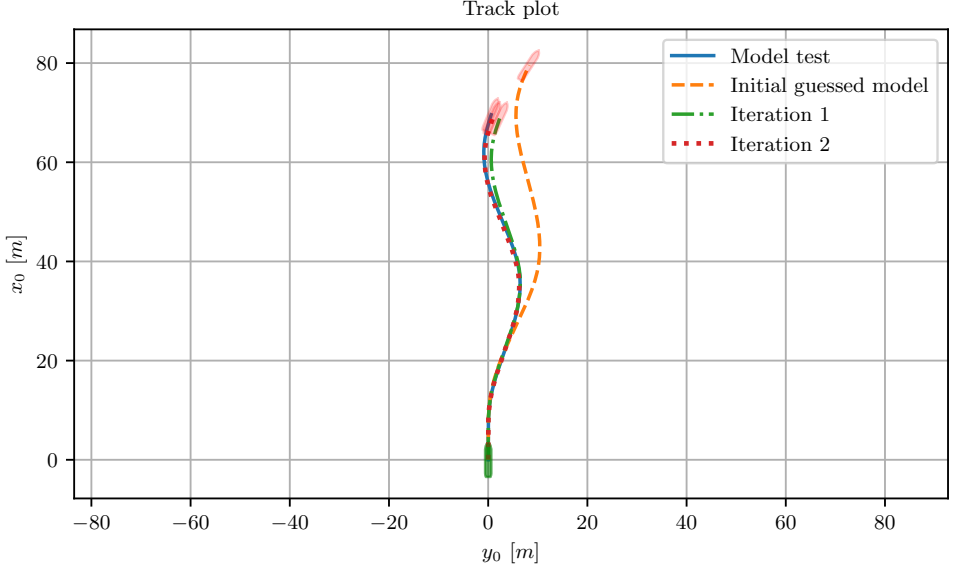


Figure 3.2: Simulation with: initial model and first and second iteration of the parameter estimation method.

3.2.1 Inverse dynamics and regression

Each manoeuvring model has some hydrodynamic functions $X_D(u, v, r, \delta, thrust)$, $Y_D(u, v, r, \delta, thrust)$, $N_D(u, v, r, \delta, thrust)$ that are defined as polynomials. The hydrodynamic derivatives in these polynomials can be identified with force regression of measured forces and moments. The measured forces and moments are usually taken from captive model tests (CMT), planar motion mechanism (PMM) tests, or virtual captive tests (VCT). However, motions are recorded when the ship is free in all degrees of freedom. Hence, forces and moments causing ship motion must be estimated by solving the inverse dynamics problem. The inverse dynamics problem is solved by restructuring the system equation (Eq. (2.7)) to get the hydrodynamics functions on the left-hand side. If the mass and inertia of the ship with added masses: $X_{\dot{u}}$, $Y_{\dot{v}}$, $Y_{\dot{r}}$, $N_{\dot{v}}$, and $N_{\dot{r}}$ are known; the forces in the Prime system can be calculated using Eq. (3.3), Eq. (3.4), and Eq. (3.5). These forces can be used to regress the hydrodynamic derivatives through the ordinary least square (OLS) method. If the added masses are unknown, they can be calculated using potential flow methods or semi-empirical methods (Appendix A).

$$X_D'(u', v', r', \delta, thrust') = -X_{\dot{u}}'\dot{u}' + \dot{u}'m' - m'r'^2x'_G - m'r'v' \quad (3.3)$$

$$Y_D'(u', v', r', \delta, thrust') = -Y_{\dot{r}}'\dot{r}' - Y_{\dot{v}}'\dot{v}' + \dot{r}'m'x'_G + \dot{v}'m' + m'r'u' \quad (3.4)$$

$$N_D'(u', v', r', \delta, thrust') = I_z'\dot{r}' - N_{\dot{r}}'\dot{r}' - N_{\dot{v}}'\dot{v}' + \dot{v}'m'x'_G + m'r'u'x'_G \quad (3.5)$$

An example that includes forces calculated with inverse dynamics from motions in a turning circle test can be seen in Figure 3.3. The forces have been converted to SI units.

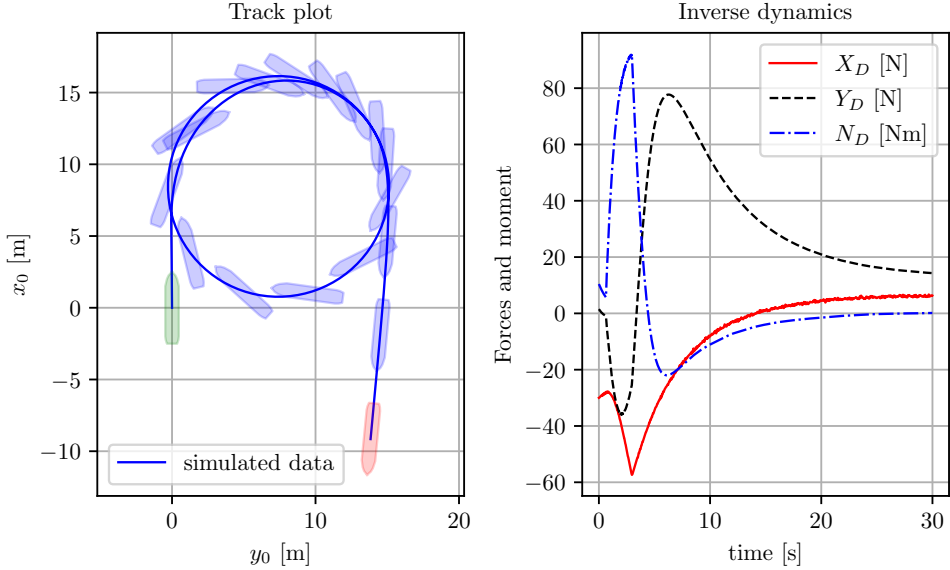


Figure 3.3: Forces and moments calculated with inverse dynamics on data from a turning circle test.

3.2.2 Data cleaning

It is possible to do an exact parameter estimation on flawless (simulated) data with no noise (see Paper 2). However, such data from physical experiments does not exist in reality. The measured data will always contain process noise and measurement noise. In order to mitigate the effects of noise, the data is pre-processed using the extended Kalman filter (EKF) (Brown and Hwang 1997) and the Rauch Tung Striebel (RTS) smoother (Rauch et al. 1965), which are both presented below. EKF is an extension of the Kalman filter (KF) that is used to work on nonlinear systems such as the manoeuvring models. The premise is that noise can be neglected if it has no rational physical explanation. For instance, if noisy measurement data would be completely correct, that would mean that large ship vibrations must have originated from large high frequency forces considering the large mass of the ship. A prior understanding of the dynamics suggests that these forces are not present. Therefore, the noise should be considered as measurement noise and should be removed. Low-pass filtering is commonly used to remove noise; motions above a cutoff frequency are considered unphysical measurement noise. The problem with low-pass filtering is that choosing the cutoff frequency is difficult. It is often either too low (removing some of the signal) or too high (keeping some unfiltered measurement noise in the data). The Kalman

filter has a predictor model, a manoeuvring model in this case, that continuously estimates the system's state that runs parallel with the measurement data. The filter estimates the current state as a combination of the measurement data and the predictor model estimate based on the possible validity of the data and the model. If the data has low noise, the estimate is closer to that data. Conversely, if the model provides very accurate predictions, then that estimate is closer to the model. The system's inverse dynamics require everything about the state (positions, velocities, and accelerations) to be known. Only positions are known from the measurements, but the velocities and accelerations are instead estimated by the EKF. The EKF is recursive and can be ran online; it continuously makes new estimates as new measurements arrive. The EKF uses passed measurements to estimate states in the near future. This property is commonly used for online applications such as autopilots or autonomous ships. This restriction is unnecessary for the estimation for already existing data, where an entire time series of existing measurements is available. The knowledge of both past and future data can be used to improve the filter. An EKF filter can include future time steps by adding the RTS smoother after the filter. The RTS smoother is an algorithm that runs the EKF backward to account for future time steps. The used EKF recursive algorithm used is summarized in the pseudo-code below (Brown and Hwang 1997).

Algorithm 3.1 (Discrete-time extended Kalman filter)

Inputs Initial values: $x_0, P_0, C_d, R_d, Q_d, E_d$

Output Estimated states: \hat{x} , estimated state covariances \hat{P}

1. Initial values:
 1. $\hat{x}[0] = x_0$
 2. $\hat{P}[0] = P_0$
 2. For k in n measurements (time steps)
 1. KF gain
 1. $K[k] = \hat{P}[k]C_d^T (C_d\hat{P}[k]C_d^T + R_d)^{-1}$
 2. $I_{KC} = I_n - K[k]C_d$
 2. Update
 1. State corrector $\hat{x}[k] = \hat{x}[k] + K[k](y - C_d\hat{x}[k])$
 2. Covariance corrector $\hat{P}[k] = I_{KC} \cdot \hat{P}[k]I_{KC}^T + K[k]R_dK^T$
 3. Predict
 1. State predictor $\hat{x}[k+1] = \hat{x}[k] + h \cdot \hat{f}(\hat{x}[k], c[k])$
 2. Covariance predictor $\hat{P}[k+1] = A_d[k]\hat{P}[k]A_d[k]^T + E_dQ_dE_d^T$
-

Here, n is number of states (6 in this case), I_n is an $n \cdot n$ identity matrix. The transition matrix is calculated for each iteration using a Jacobian of the transition model:

$$A_d[k] = I + h \left. \frac{\partial f(x[k], c[k])}{\partial x[k]} \right|_{x[k] = \hat{x}[k]} \quad (3.6)$$

This part and the fact that the nonlinear transition model is used directly as the predictor are the extension part of the EKF compared to the linear KF. Please note the linear approximation in Eq. (3.6) around the current state. This approximation can cause stability problems if the real system and the linearized system deviates too much, when large time steps are used on a very nonlinear system. The Unscented Kalman Filter, which was used in Revestido Herrero and Velasco González (2012), is an alternative that can be used in these situations.

The output from the filter contains the estimated states: \hat{x} and estimated state covariance matrix \hat{P} . \hat{x} represent the most likely estimates, but the estimates have uncertainty that is expressed in \hat{P} . The state of the system is described by the ships position, heading, velocities and yaw velocity:

$$x = [x_0, y_0, \psi, u, v, r]^T \quad (3.7)$$

The initial state x_0 is taken as the mean value of the first five measurements, where the velocities are estimated with numeric differentiation.

C_d selects the measured states (x_0, y_0, ψ):

$$C_d = h \begin{bmatrix} 1 & 0 & 0 & 0 & 0 & 0 \\ 0 & 1 & 0 & 0 & 0 & 0 \\ 0 & 0 & 1 & 0 & 0 & 0 \end{bmatrix} \quad (3.8)$$

E_d selects the hidden states (u, v, r):

$$E_d = h \begin{bmatrix} 0 & 0 & 0 \\ 0 & 0 & 0 \\ 0 & 0 & 0 \\ 1 & 0 & 0 \\ 0 & 1 & 0 \\ 0 & 0 & 1 \end{bmatrix} \quad (3.9)$$

where h is the discrete time step, R_d describes the covariance matrix of the measurement, Q_d is the covariance matrix of the process model, and P_0 is the initial state covariance. Selecting good values for these three matrices is the most complicated part of getting the EKF to work well. The amount of expected measurement noise in the data should be inserted in to R_d , and the amount of error generated by the process model (manoeuvring model) needs to be estimated in Q_d . The choices for these matrices depend on the reliability of the present data and the present process model.

3.2.3 Regression

Finding the hydrodynamic derivatives can be defined as a linear regression problem following the "derivation approach" (see subsection 3.1.1):

$$y = X\gamma + \epsilon \quad (3.10)$$

The label vector y and feature matrix X in the regression problem in Eq. (3.10) can be calculated if model for the hydrodynamic forces is assumed. For example: the label in the regression of the surge degree of freedom for the MAVMM can be calculated using the inverse dynamics force, which is expressed with primed units:

$$y = -X_u \dot{u}' + \dot{u}' m' - m' r'^2 x_{G'} - m' r' v' \quad (3.11)$$

The feature matrix X is expressed as:

$$X = [\text{thrust}' \quad u' \quad \delta^2 \quad r'^2 \quad u'^2 \quad r'v'] \quad (3.12)$$

The hydrodynamic derivatives in the γ vector (Eq. (3.13)) can be estimated with ordinary least squares (OLS) regression.

$$\gamma = \begin{bmatrix} X_T \\ X_u \\ X_{\delta\delta} \\ X_{rr} \\ X_{uu} \\ X_{vr} \end{bmatrix} \quad (3.13)$$

In this regression, the hydrodynamic derivatives are treated as Gaussian random variables. The hydrodynamic derivatives in the manoeuvring model are usually estimated as the mean value of each regressed random variable, which is the most likely estimate. The regression result can be expressed with a multivariate Gaussian distribution, which is defined by the regression's mean values and covariance matrix. The multivariate Gaussian distribution can be used to conduct Monte Carlo simulations in the study of alternative realizations of the regression.

Strong multicollinearity is a documented problem for the manoeuvring models (Luo et al. 2016; Wang and Zou 2018). The thrust coefficient X_T in the hydrodynamic function X_D in Eq. (2.14) introduces multicollinearity to the regression. This coefficient can instead be calculated from the thrust deduction factor t_{df} :

$$X_T = 1 - t_{df} \quad (3.14)$$

The X_T coefficient is excluded from the regression by moving it to the left-hand side of the regression equation Eq. (3.10):

$$y - X_T \cdot \text{thrust} = X\gamma + \epsilon \quad (3.15)$$

Rudder coefficients (Y_R) from Y_D equation Eq. (2.15), such as Y_δ and $Y_{\delta T}$, have also been excluded by assuming a connection with their N_D equation counterpart through the rudder lever arm x_r :

$$Y_R = \frac{N_R}{x_{r'}} \quad (3.16)$$

3.3 Model development process

The aim of developing a manoeuvring model with parameter estimation is to develop a model that can generalize outside the known data. The method presented in this thesis is assessed with the hold-out evaluation (Sammut and Webb 2017). The data in this evaluation is divided into three sets: the training set, the validation set, and the test set as seen in Figure 3.4.

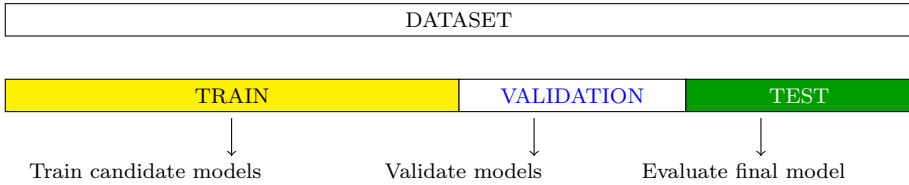


Figure 3.4: Model development process with hold-out evaluation.

The purpose of the training set is to train all the candidate models using the proposed parameter estimation method. The validation set is used to select the most effective candidate model. The training and validation sets are joined to train the selected model as the final model. The final model is used for predicting the test set, which is used to evaluate the accuracy of the model. These three sets are not divided randomly; they are divided to assess the model's extrapolation ability. The data sets are therefore split to have the smallest yaw rates, drift-angles, and rudder-angles in the training set; the medium values in the validation set; and the largest values in the test set. Examples of this can be seen for the two test cases in this thesis in Figure 4.16 and Figure 4.10 in the next chapter.

Summary and discussions of appended papers

This chapter presents a summary of the appended papers, which includes research activities and a selection of the most relevant results including a model for the roll motion in Paper 1 and, a manoeuvring model with a high level of generalization in Paper 2.

4.1 Summary of Paper 1

"Analysis of roll damping model scale data"

System identification of ship roll motion, which includes roll damping and stiffness, is developed in Paper 1. Parametric roll was observed by Froude (1861) and has been a focus of the marine research community since the early 1950s (Galeazzi et al. 2013); it has received even more attention since France et al. (2001) demonstrated that the APL China casualty in 1998, where a post-Panamax C11 class container ship lost almost a third of its containers, was most likely caused by head sea parametric rolling. The damping of roll motion plays an important role in these phenomena. Previous literature demonstrates that the relatively small difference in the roll damping prediction obtained with small method variation may contribute to the difference between severe roll angles and much less noticeable motions (Söder et al. 2019a).

The objective of Paper 1 was to improve the roll damping predictions for modern ships. The roll damping was studied using time series data from 250 (see Figure 4.1) roll decay tests (see section 2.1) assembled by the Maritime Dynamics Laboratory at SSPA Sweden AB (www.sspa.se). The work was divided into the following sub tasks (also summarized in Figure 4.2):

- Find the mathematical model that is the best representation of the roll motion.
- Identify the parameters in this model for all the tests.
- Compare the identified parameters with state of art predictions.
- Develop a generic roll damping model for all ships using the identified parameters.
 - Grey-box model
 - Black-box model

System identification on the time series from the roll decay database was performed with the linear (Eq. (2.3)), quadratic (Eq. (2.4)), and cubic models (Eq. (2.5)). Estimated roll damping parameters were used to build a roll damping database. The database could be compared to corresponding predictions with the simplified Ikeda's method (Kawahara et al. 2011), which is the state of art prediction for ship roll damping. The generic roll damping model was developed as a grey-box model and a black-box model.

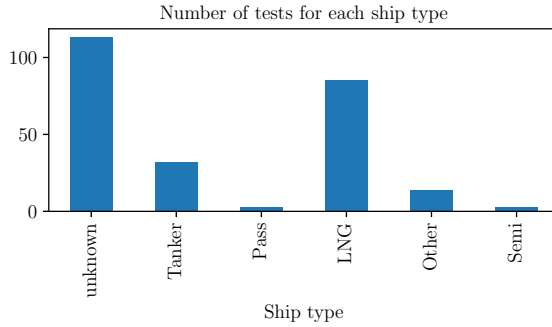


Figure 4.1: Number of tests per ship type.

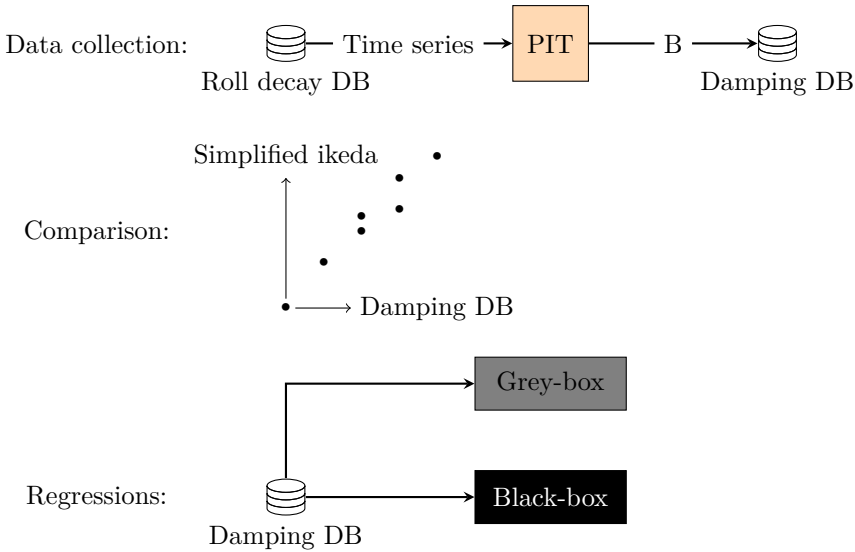


Figure 4.2: Overview of the work conducted for Paper 1.

4.1.1 Best mathematical model for the roll motion

System identification on the linear, quadratic, and cubic models was conducted using both the “integration approach” (subsection 3.1.2) and the “derivation approach” (subsection 3.1.1) where the best parameter estimations were obtained using the “integration approach”. Results from the simulations with the identified models (from one of the roll-decay tests) are presented in Figure 4.3. The cubic and quadratic models reproduce the model test well, and the linear model is too simple to provide an accurate representation for both smaller and larger roll angles. The amplitude decrement ϕ_a and roll damping B for each oscillation can be visualized, as seen in Figure 4.4. The goodness of fit for the linear, quadratic, and cubic models can be

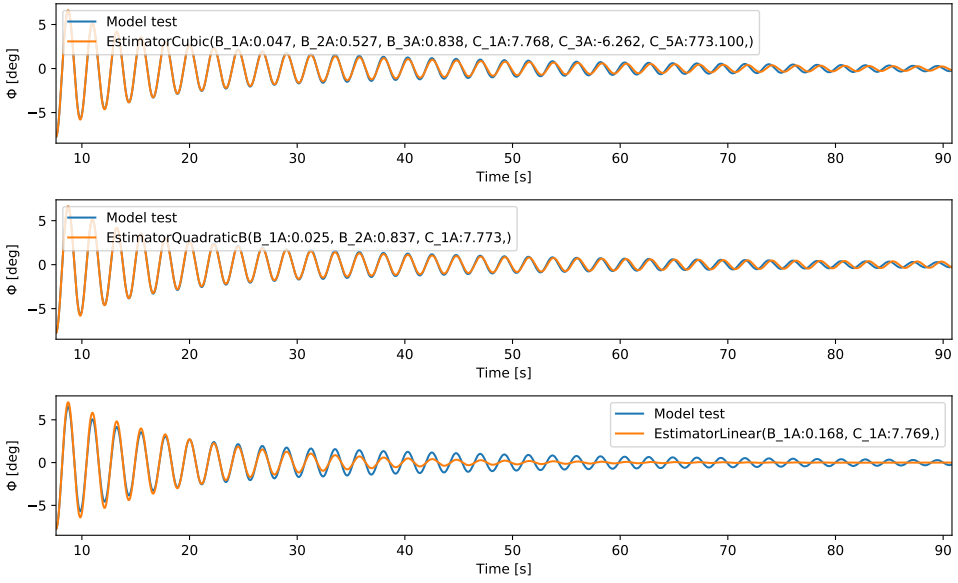
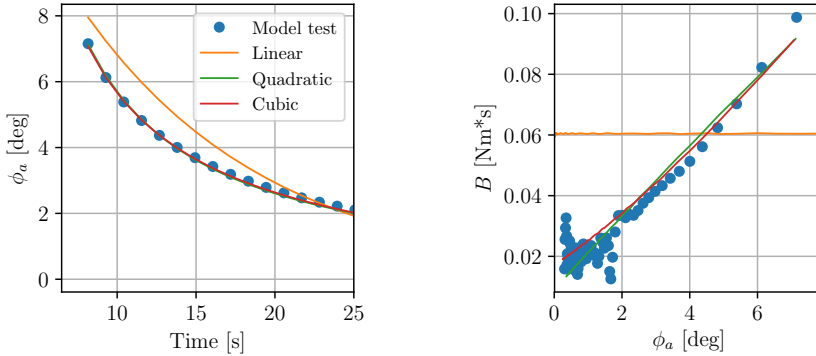


Figure 4.3: Roll decay estimation with identified cubic, quadratic, and linear models.



(a) Amplitude decrements.

(b) Dampings.

Figure 4.4: Roll decay model test, linear-, quadratic- and cubic-model.

expressed using the coefficient of determination:

$$R^2 = 1 - \frac{\sum_{i=1}^n (\phi_i - \hat{\phi}_i)^2}{\sum_{i=1}^n (\phi_i - \bar{\phi})^2} \quad (4.1)$$

where ϕ_i is the model test roll angle at time step i , $\bar{\phi}$ is the mean roll angle from the model test, and $\hat{\phi}_i$ is the predicted roll angle (with the linear, quadratic, or cubic model). The average goodness of fit R^2 was 0.995 for the cubic model, 0.993 for the quadratic model, and 0.986 for the linear model. These values indicate that the quadratic model is almost as useful as the cubic model for describing the roll motion. The quadratic model, with fewer parameters than the cubic model, is expected to have a higher level of generalization at the same accuracy and is therefore selected as the best mathematical model for the roll motion.

4.1.2 Comparison with Ikeda's method

Ikeda's method divides roll damping into five damping components: the friction component B_F , the eddy component B_E , the lift component B_L , the wave component B_W , and the bilge keel component B_{BK} , as in the following Eq.(4.2),

$$B_{44} = B_F + B_E + B_L + B_W + B_{BK} \quad (4.2)$$

where the wave and eddy components require strip-theory based hydrodynamic analysis to obtain the ship's shape coefficients. The hydrodynamic analysis requires the ship's exact hull geometry. Building the geometry model and performing the strip-theory based hydrodynamic analysis are time-consuming. A ship's hull geometry is not always available for such purposes. A simplified Ikeda's method (SI-method) proposed by Kawahara et al. (2011) is used in Paper 1 to calculate all the damping components, which include the eddy component B_E and the wave component B_W . The semi-empirical formulas describe four of the five roll damping components at motion frequency ω for a given roll amplitude ϕ_a at zero ship speed. A speed dependency was introduced by adding a fifth damping term B_L and a speed correction to B_W and B_E , as described in Ikeda (1979), giving a function:

$$(B_F, B_W, B_E, B_{BK}, B_L) = f(L_{pp}, beam, C_b, A_0, OG, \phi_a, BK_L, BK_B, \omega, T, V) \quad (4.3)$$

The formulas within f can be expressed as Ikeda (1979) and Kawahara et al. (2011) with the implementation in Alexandersson (2022b). It should be noted that this method is only efficient for the estimation of the roll damping of ships within the boundaries (Kawahara et al. 2011):

$$\begin{cases} 0.5 \leq C_b \leq 0.85, & 0 \leq \hat{\omega} \leq 1.0, & 0.9 \leq A_0 \leq 0.99, \\ 2.5 \leq Beam/T \leq 4.5, & 0.01 \leq BK_B/Beam \leq 0.06, \\ -1.5 \leq OG/T \leq 0.2, & 0.05 \leq BK_L/L_{PP} \leq 0.4. \end{cases} \quad (4.4)$$

The total roll damping is predicted as the sum (Eq. (4.2)) of the damping contributions (Eq. (4.3)). This damping can be compared with the linearized equivalent damping B_e , which is calculated for a certain roll angle ϕ_a with the identified roll damping parameters B_1 and B_2 (Himeno 1981),

$$B_e = B_1 + \frac{8B_2\omega_0\phi_a}{3\pi} \quad (4.5)$$

The B_e non-dimensional form of the coefficient can be used according to Himeno (1981). The non-dimensional equivalent for the linear damping coefficient is \hat{B}_e . This form is more convenient when comparing roll damping for different ships,

$$\hat{B}_e = \frac{B_e}{\rho \nabla \text{Beam}^2} \sqrt{\frac{\text{Beam}}{2g}}, \quad (4.6)$$

where ρ , ∇ , and Beam stand for fluid density, displacement volume, and breadth of a ship, respectively. Prediction error plots of \hat{B}_e from the simplified Ikeda's method and identified damping from the model tests are presented in Figure 4.5a. In this figure, a comparison of predictions with roll amplitudes in the range of 0 to 10 degrees is displayed for all ships with no limits and for ships within the limits of the method (Eq. (4.4)). The R^2 values of the predictions are displayed in Table 4.1. There is reasonable agreement between the predicted roll damping and model tests for ships within the limits. There is very poor agreement for ships outside the limits. It should be noted that most of the points are outside the limits of the method.

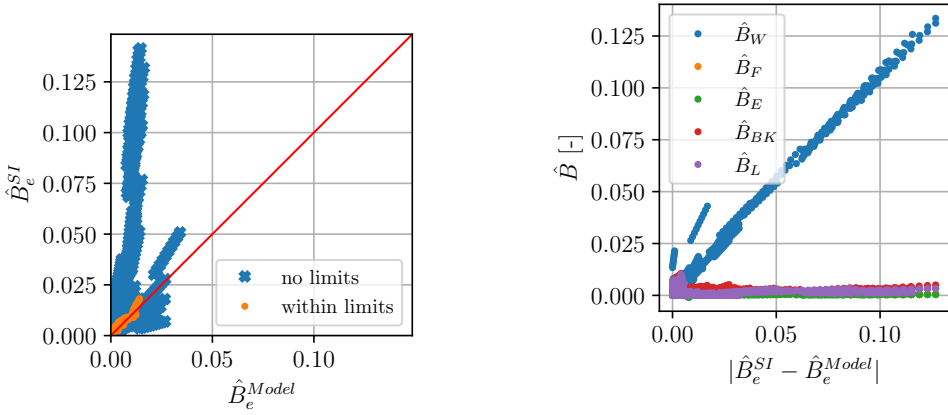
Table 4.1: Validation of SI within and outside limits.

	R^2	Number of points
SI no limits	-46.35	1470
SI within limits	0.83	120

The largest contribution to the error in the predictions comes from the wave damping B_W , as seen in Figure 4.5b. A comparison of the simplified Ikeda's method and the original Ikeda's method was carried out in Paper 1; the comparison was used to determine whether the observed deviations are the result of extrapolation or inherent to the original method. In Ikeda's method, more extensive knowledge of the ship hull geometry is needed in order for B_W to be calculated with a strip method and B_E to be calculated with sectional Lewis coefficients. It was possible to collect the required hull inputs for 15 ships in the database. These ships were used in 50 of the reference roll decay tests; all but one of the tests exceed the limits. Ikeda's method has much more agreement for these exceeding model tests according to Figure 4.5c and the calculated R^2 in Table 4.2.

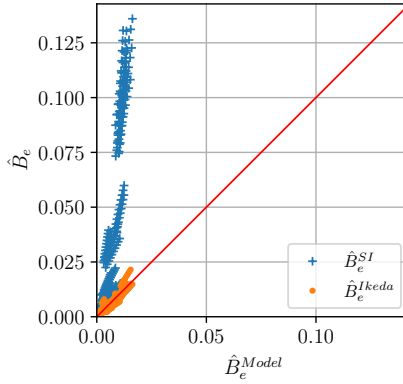
Table 4.2: Validation of SI and Ikeda.

	R^2	Number of points
Ikeda	0.84	500
SI no limits	-127.95	500



(a) The simplified Ikeda's method within and outside its limits.

(b) Residuals vs. components.



(c) Comparison of simplified and original Ikeda's method and model tests.

Figure 4.5: Prediction error plots.

4.1.3 Generic roll damping model

A serial grey-box model for ship roll damping (see Figure 4.6) is also developed in Paper 1. This is expanding the system identification by not only focusing on one ship, but all modern ships. The simplified Ikeda's method (Kawahara et al. 2011) is used as the white-box model, which is combined with the following black-box correction model.

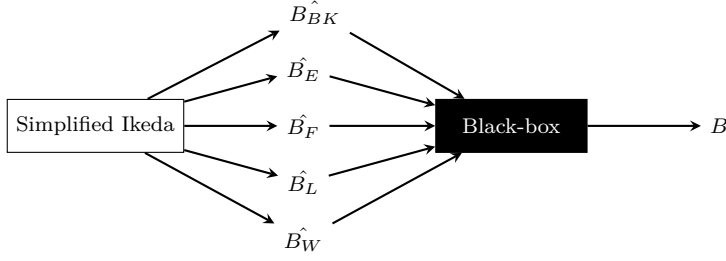


Figure 4.6: Grey-box model to predict roll damping.

The roll damping data set, obtained from the roll motion investigation, is intended to train the black-box component of the grey-box model. The black-box correction model of the output components from the simplified Ikeda's method is displayed in (Eq. (4.7)),

$$\hat{B}_e = 1.106\hat{B}_{BK} - 0.9124\hat{B}_E + 4.282\hat{B}_F + 0.7457\hat{B}_L + 0.1844\hat{B}_W + 0.004999\phi_a - 0.0005097 \quad (4.7)$$

Major corrections to the skin friction damping \hat{B}_F and wave damping \hat{B}_W are included in this expression. The corrections are included because the simplified Ikeda's method is not very accurate for this dataset; most of the ships in the dataset exceeded the limits of the method. A pure black-box model is also developed in Paper 1 (see Eq. (4.8)),

$$\begin{aligned} \hat{B}_e = & -0.02578A_0V - 0.02705BK_BV + \\ & 0.008993BK_LV - 0.03191C_bV - 0.2028OGV + \\ & 0.003472V^2 + \\ & 0.004234V\hat{\omega}_0 - 0.002591V\phi_a - 0.008384Vbeam + \\ & 0.05048V + \\ & 0.007814\hat{\omega}_0^2 + \\ & 0.03882\hat{\omega}_0\phi_a - 0.001069 \end{aligned} \quad (4.8)$$

where non-dimensional frequency $\hat{\omega}_0$ is calculated with Eq. (4.9) (Himeno 1981),

$$\hat{\omega}_0 = \frac{\sqrt{2}\omega_0\sqrt{\frac{beam}{g}}}{2} \quad (4.9)$$

Over-fitting data is a concern when constructing a regression model from a data set. Including too many parameters or allowing the order of the model to be too high would provide a very accurate representation of the present roll damping data. However, such a representation would be accompanied by major extrapolation errors when the model is used for other data. The generalization of the model can be assessed with a hold-out evaluation by using K-fold cross validation (Mosteller and Tukey 1968) (Figure 4.7). The data has been divided into five smaller sets (folds).

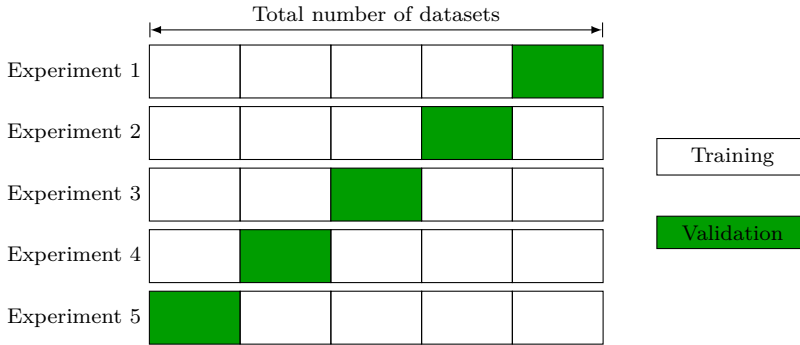


Figure 4.7: K-fold cross validation.

Four of the folds are used to train the model, and the fifth fold is used for testing (validation). Validation consists of calculating the coefficient of determination R^2 for the fitted model. Validation is completed for all five possible train-test combinations. The folds are randomly constructed with the restriction that all data for a particular ship must be in the same fold. Five folds are randomly generated 20 times, which gives 100 values of R^2 from the train-test-procedure for each model. The mean values and standard deviation of these 100 values of R^2 are displayed in Table 4.3. The mean and standard deviation of R^2 simplified Ikeda's method in this table were calculated directly instead of using cross validation because they do not rely on the SSPA data.

Table 4.3: Statistics from cross validations with all models.

model	$E[R^2]$	$std(R^2)$
Simplified Ikeda corrected	0.75	0.16
New regression	0.77	0.09

4.2 Summary of Paper 2

"System identification of vessel manoeuvring models"

In order to expand the modelling complexity and uncertainty from Paper 1, system identification of the surge, sway, and yaw degrees of freedom is studied in Paper 2. The dynamics are assumed to be described by a ship manoeuvring model (section 2.2). The system identification method proposed in Paper 2 was validated on two case study ships: the wPCC (Figure 4.8) and the KVLCC2 (Figure 4.9). The models are developed using the process described in section 3.3. Consequently, both test cases aim to predict turning circle maneuvers. The primary dimensions of the two case study ship models are listed in Table 4.4, with explanations in Table 4.5. The wPCC is a wind-powered car carrier tested at SSPA (Alexandersson 2022c). This twin screw ship with large rudders has good course stability and symmetric hydrodynamic manoeuvring forces. The KVLCC2 model test data from the Hamburg ship model basin (HSVA) and Maritime research institute Netherlands (MARIN) was made available by the SIMMAN2008 conference (Stern et al. 2011). This single screw ship has less course stability than the wPCC test case, and manoeuvring forces are unsymmetrical due to the single propeller. This instability makes it an appropriate second test case with parameter estimation on an unsymmetrical model.



Figure 4.8: wPCC tested at SSPA. Copyright 2020 by SSPA.

Table 4.4: Main dimensions of test case ship models.

	B [m]	D [m]	L [m]	LCG [m]	N_p	c [m]	α	∇ [m ³]	k_{zz}	m [kg]	w_{p0}	x_p [m]	x_r [m]
WPCC	0.95	0.12	5.01	0.0	2	0.21	41.2	0.44	0.25	441	0.15	-2.42	-2.42
KVLCC2 (HSVA)	1.27	0.2	7.0	0.24	1	0.46	45.7	3.27	0.25	3272	0.4	-3.39	-3.5



Figure 4.9: Ship model used in HSVA and MARIN model tests. Copyright HSVA.

Table 4.5: List of main dimensions symbols.

symbol	description
B	Beam
D	Propeller diameter
L	Length between perpendiculars
L_{CG}	Distance $L/2$ to centre of gravity
N_p	Number of propellers
T	Draught
α	Scale factor
∇	Volume displacement
k_{zz}	Radius of gyration / L
m	Mass (excluding added mass)
w_{p0}	Wake fraction
x_p	Longitudinal position of propeller
x_r	Longitudinal position of rudder

The parameter estimation method requires an initial guessed linear manoeuvring model. The initial models for the two test cases have hydrodynamic derivatives (Table 4.6) that are calculated with semi-empirical formulas (Appendix A) sourced from Brix (1993).

Table 4.6: Initial guessed derivatives in linear models (times 1000).

	N_δ	N_r	$N'_\dot{r}$	N_v	$N'_\dot{v}$	$X'_\dot{u}$	Y_δ	Y_r	$Y'_\dot{r}$	Y_v	$Y'_\dot{v}$
WPCC	-1.5	-1.719	-0.299	-3.184	-0.128	0.179	3.0	2.402	-0.303	-9.713	-6.109
KVLCC2 (HSVA)	-1.5	-3.415	-0.822	-8.707	-1.166	1.05	3.0	4.305	-1.271	-25.266	-15.846

4.2.1 The wPCC test case

The wPCC test case focuses on predicting forces and moments from the ship hull and the rudders. The propeller force is not part of the prediction model; it is obtained from the model test measurements. In the model development process (section 3.3), the model test data used for modelling is split into the training test, the validation test, and the test data sets (also presented in Figure 4.10),

- The training dataset: self-propulsion, pull-out tests, and zigzag10/10 tests to starboard and port.
- The validation dataset: three zigzag20/20 tests.
- Test dataset: one turning circle test.

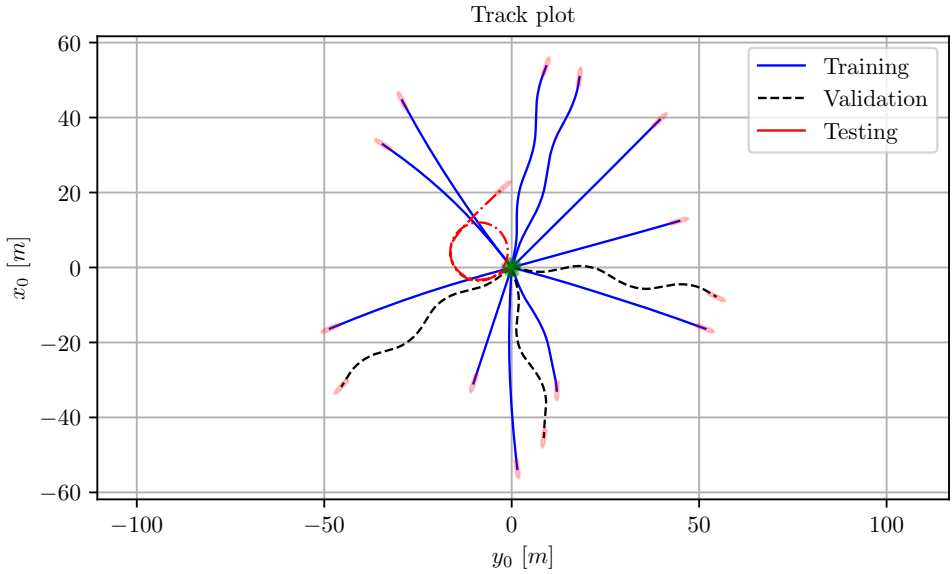


Figure 4.10: wPCC training, validation and testing datasets.

If the manoeuvring model built by the proposed method based on a series of model tests (including ZigZag10/10 and 20/20 to port and starboard as well as the self-propulsion and pull out test) (IMO 2002) can predict the turning circle maneuver, then it is a capable model. The linear model (LVMM) was ruled too simple for the wPCC. Only the AVMM and MAVMM were considered possible manoeuvring models in the model selection. Forces and moment predicted for the validation dataset, with the manoeuvring models fitted with proposed parameter estimation on the training set, are presented in Figure 4.11. The fitted AVMM over-predicts the forces by far. The over-prediction of forces with the AVMM can be explained by the major problems with multicollinearity that were encountered when applying the parameter estimation method to the wPCC data.

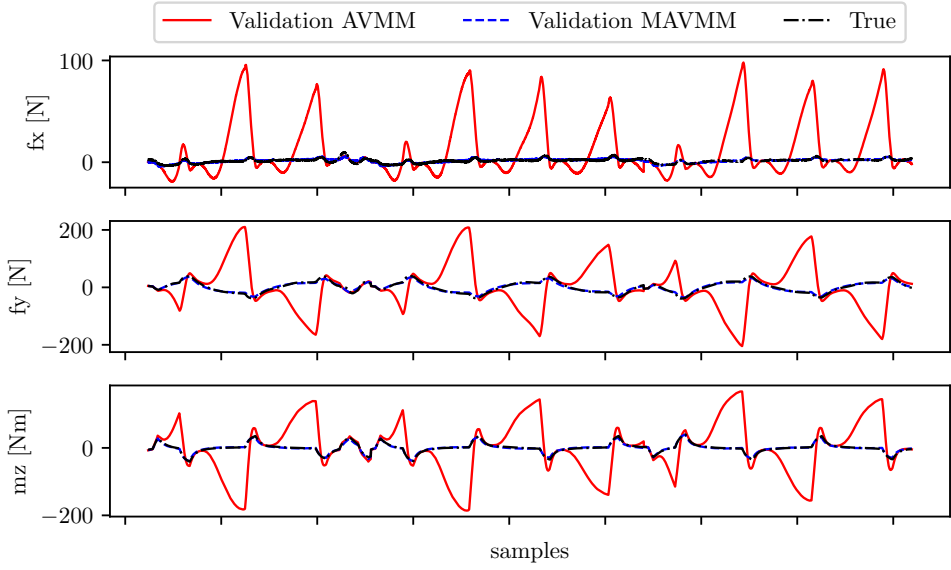


Figure 4.11: Validation of force models for wPCC ZigZag20/20.

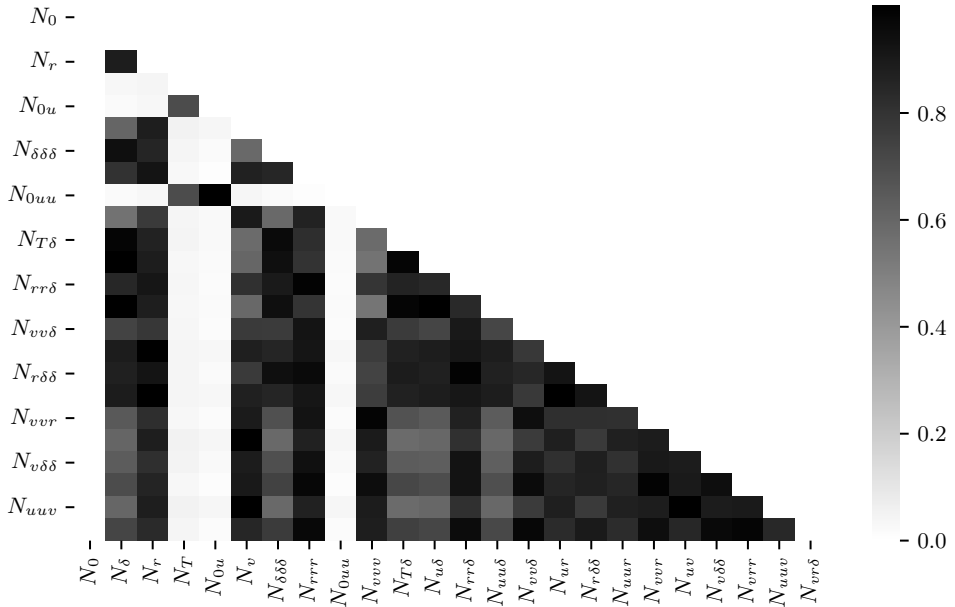


Figure 4.12: Absolute correlation between the features in the wPCC yaw moment regression of AVMM.

The absolute correlation coefficient between the features in the wPCC yaw moment regression is presented in Figure 4.12. Most of the coefficients have a very high absolute correlation (indicated in black). Some of the regressed hydrodynamic derivatives in the AVMM also have substantial values and large degrees of uncertainty. Therefore, simulations of the validation cases are only possible using the MAVMM. The simulations are displayed for one of the ZigZag20/20 validation cases in Figure 4.13. The MAVMM was therefore selected as the most appropriate model for the wPCC in

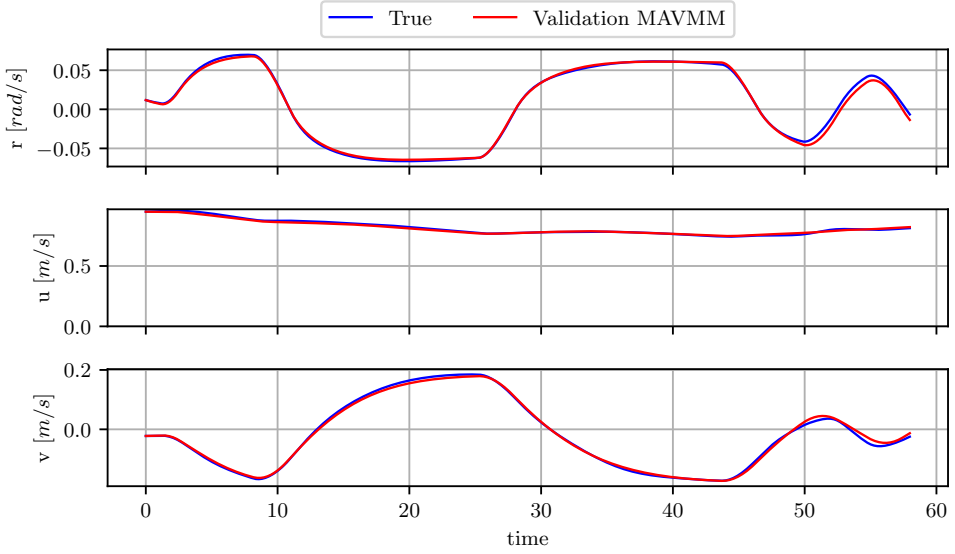


Figure 4.13: Validation with simulations for wPCC ZigZag20/20.

the validation step of the model development process. This model was retrained on the joined test and validation data set to obtain the final prediction model which was used to predict the turning circle test data set. Advance and tactical diameter (IMO 2002) from the prediction differs by 4% and 1% from the model test data, as seen in Table 4.7.

Table 4.7: wPCC Predicted turning circle advance and tactical diameter compared to SSPA model tests and IMO limit.

	Advance [m]	Advance (IMO) [m]	Tactical diameter [m]	Tactical diameter (IMO) [m]
Model test	12.82	22.57	14.76	25.07
Prediction	13.3	22.57	14.93	25.07

Results from the turning circle prediction are also presented in Figure 4.14 and Figure 4.15. Monte Carlo simulations with alternative realizations of the regression,

considering the uncertainty in the regressed parameters, are also displayed in these figures. The alternative realizations have similar simulation results to the model with mean values of the regression (black line).

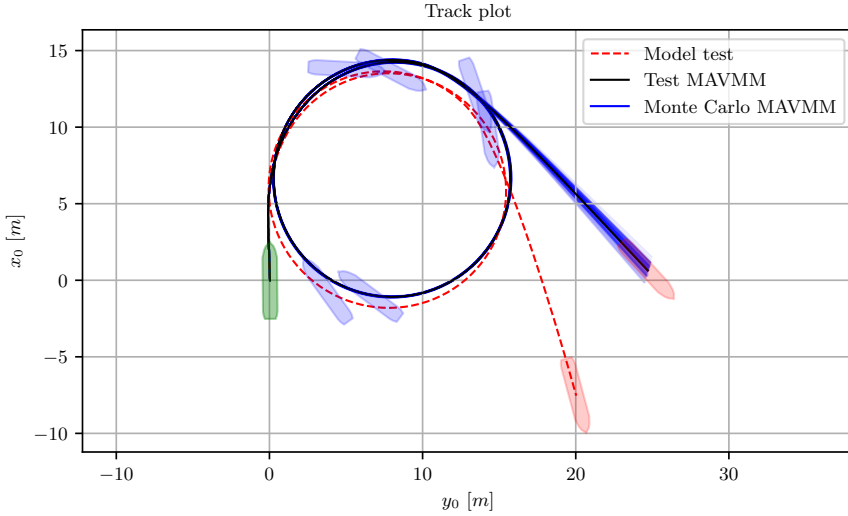


Figure 4.14: Turning circle test case for wPCC, track plots from model test and simulation.

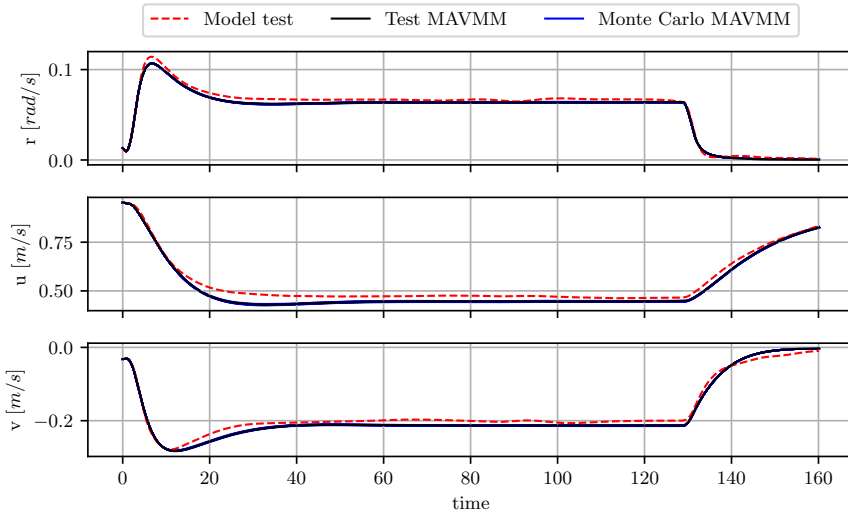


Figure 4.15: Turning circle test case for wPCC, time series from model test and simulation.

The mean values and standard error (se) of the hydrodynamic derivatives (expressed with prime units for the wPCC) obtained with parameter estimation of MAVMM (Eq. (2.17), Eq. (2.18), Eq. (2.19)) applied to all the wPCC data (including the turning circle) are displayed in Table 4.8.

Table 4.8: wPCC MAVMM derivatives (prime units times 1000).

name	mean	se	name	mean	se	name	mean	se
$X_{\delta\delta}$	-2.927	0.011	Y_{ur}	-65.507	0.082	N_{δ}	-1.993	0.002
X_{vr}	-7.737	0.066	Y_v	-20.347	0.016	$N_{T\delta}$	-5.392	0.599
X_{rr}	-1.413	0.026	Y_u	-0.027	0.001	N_r	-37.341	0.096
X_{uu}	20.124	0.137	Y_r	64.14	0.083	N_u	-0.003	0.0
X_u	-20.948	0.137				N_{ur}	35.525	0.096
						N_v	-0.05	0.004
						$N_{vv\delta}$	-19.051	0.054

4.2.2 The KVLCC2 test case

The proposed system identification method is also validated using the KVLCC2 case study ship model. The propeller is in the manoeuvring model for this test case (instead of only the hull and rudders, as in the wPCC test case) so that the entire ship can be simulated without additional input. The model development process, which is described in section 3.3, is applied to the KVLCC2 as well. The data has been split into training, validation, and test data sets (also seen in Figure 4.16),

- Training dataset: various zigzag tests to starboard and port from model tests carried out at HSVA for the SIMMAN2008 conference (Stern et al. 2011).
- Validation dataset: ZigZag35/5 carried out at HSVA for the SIMMAN2008 conference (Stern et al. 2011).
- Test dataset: turning circle model tests carried out at MARIN for the SIMMAN2008 conference (Stern et al. 2011)

A propeller prediction model is needed for the KVLCC2, which is developed from thrust measurements from the model tests, as described in the next section.

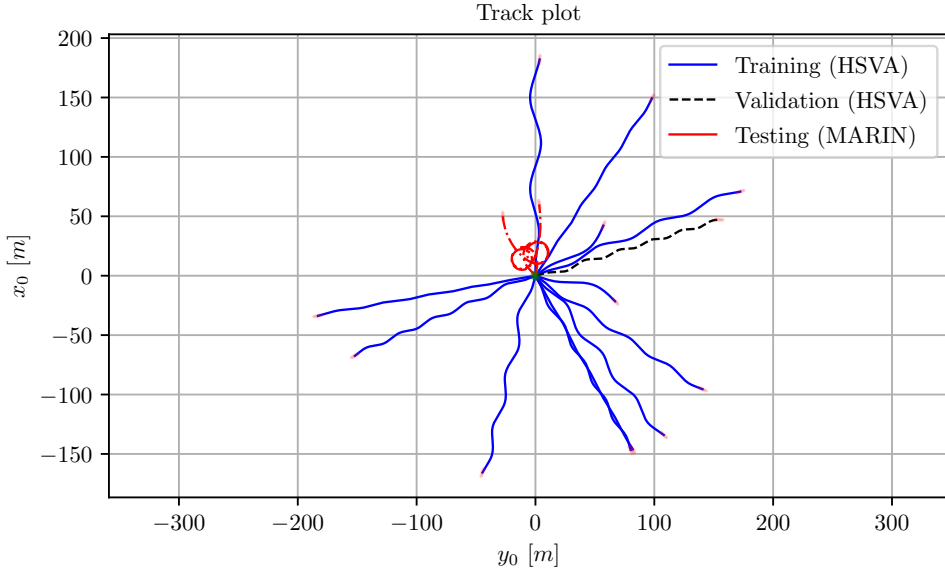


Figure 4.16: KVLCC2 training, validation and testing datasets.

The KVLCC2 propeller model

In the development of a propeller model, the coefficients in the K_T polynomial (Eq. (2.25)) were regressed from the KVLCC2 propeller characteristics from SIMMAN2008 HSVA model tests (Stern et al. 2011), as seen in Table 4.9. The propeller model was developed with cross-validation on the training and validation datasets to make the appropriate feature selection. The cross-validation study was carried out on the three candidate propeller models:

- the MMG propeller model
- the simple propeller model
- the polynomial propeller model

The training and validation sets were derived from the entire model test time series from the HSVA model tests. The model tests were randomly divided into the test and validation sets. The random training and validation sets were repeated 100 times. The Polynomial model was selected due to it having the highest accuracy. Taylor wake $w_{p0} = 0.4$ was used in all three models. The MMG model used $C_1=2.0$, $C_2=1.6$ when $\beta_p > 0$ and $C_2=1.1$ when $\beta_p \leq 0$ (Yasukawa and Yoshimura 2015). Figure 4.17 displays a small portion of the cross-validation. Coefficients of the polynomial propeller model fitted on the training and validation datasets for KVLCC2 are presented in Table 4.10.

Table 4.9: K_T polynomial coefficients.

Coefficient	Value
k_0	0.32419
k_1	-0.22091
k_2	-0.14905

Table 4.10: KVLCC2 propeller model.

	$\beta_p > 0$	$\beta_p \leq 0$
C_1	-0.1735	-0.1066
C_2	0.4589	0.0771
C_3	-1.8865	1.2958
C_4	0.0515	0.0514

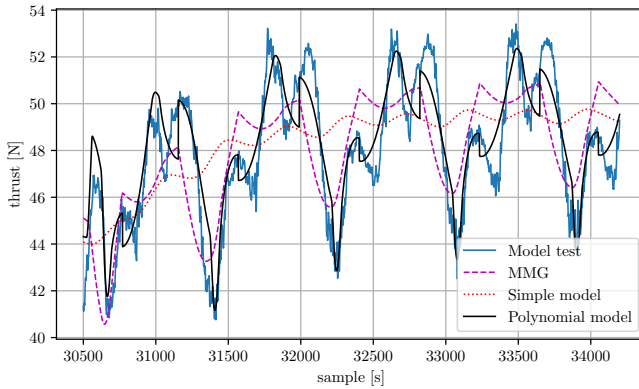


Figure 4.17: Validation of MMG, Simple, and Polynomial propeller models for KVLCC2.

KVLCC2 manoeuvring model

The linear manoeuvring model (LVMM) was ruled too simple for KVLCC2. Only the AVMM and MAVMM were considered possible manoeuvring models in the model selection. The forces and moments applied on the hull, rudder, and propeller predicted with the AVMM and MAVMM fitted with the proposed parameter estimation on the training set are displayed in Figure 4.18. The forces are accurately predicted with both manoeuvring models. The AVMM does not provide the large over-predictions that were observed from wPCC. However, the MAVMM is still slightly better and is therefore selected as the suitable manoeuvring model for the KVLCC2. Simulations of the validation cases with the MAVMM are displayed for one of the ZigZag20/20 validation cases in Figure 4.19 and Figure 4.20, where the predicted thrust is also shown.

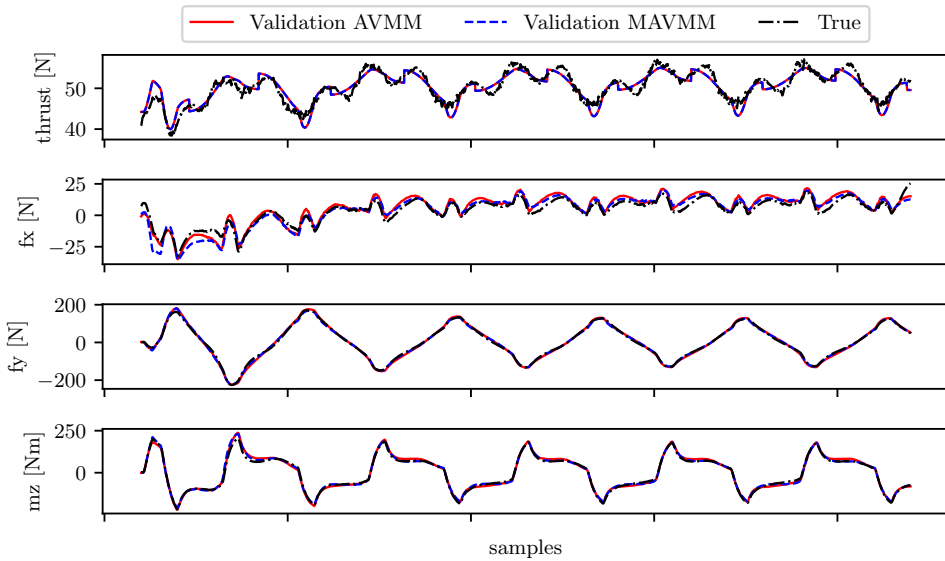


Figure 4.18: Validation of force models for KVLCC2.

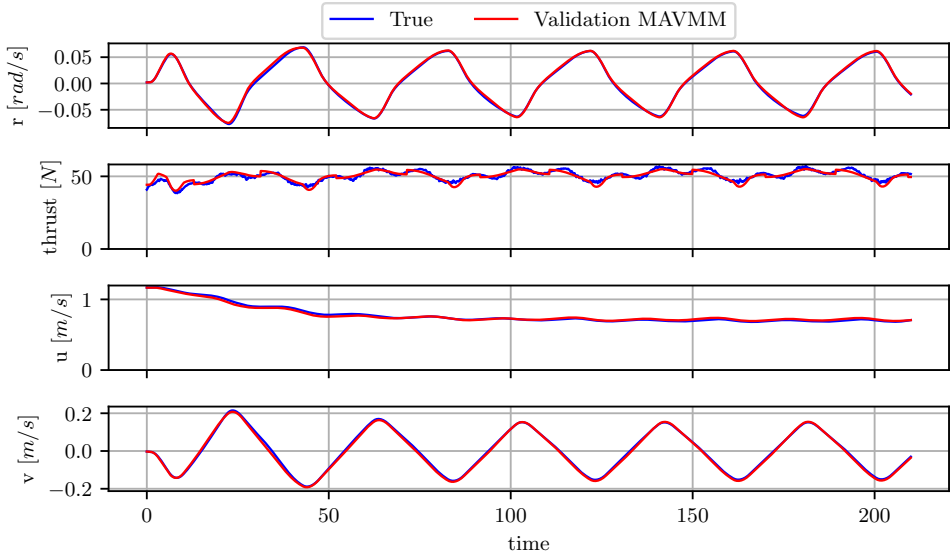


Figure 4.19: Validation with simulations for KVLCC2.

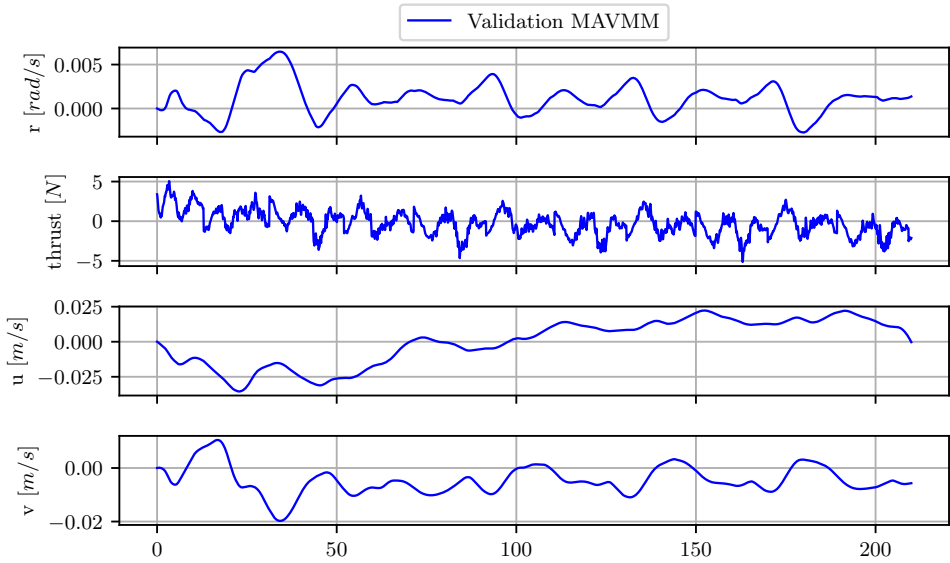


Figure 4.20: Validation error (prediction minus (-) model test) with simulations for KVLCC2.

Results from the final prediction of the turning circle test are shown in Figure 4.21, Figure 4.22 and Figure 4.23. The prediction is conducted using simulation with the MAVMM trained on the training and validation datasets. Monte Carlo simulations with alternative realizations of the regression are also displayed in this figure. The alternative realizations are very similar to the model with mean values of the regression (black line).

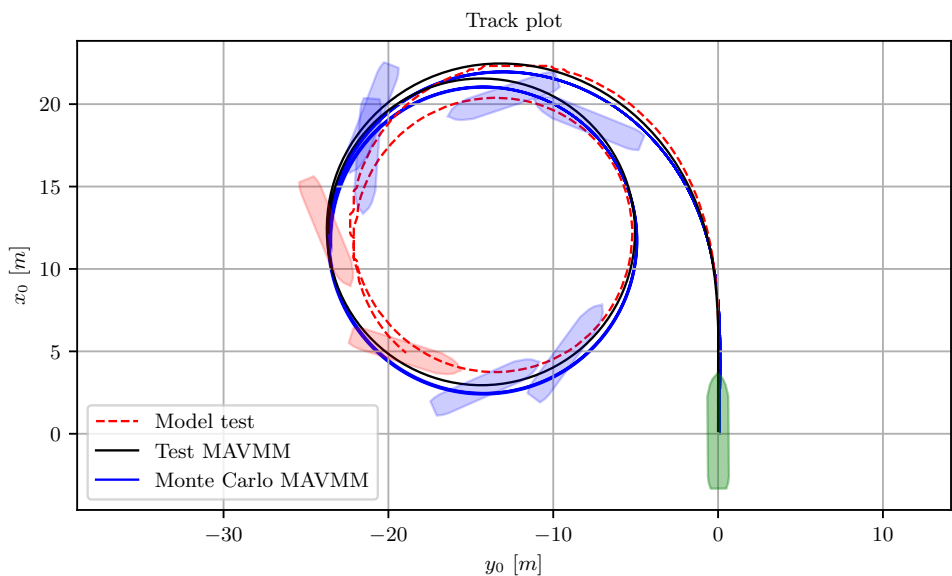


Figure 4.21: Comparison between the predicted turning circle test with MAVMM trained on HSVA data and MARIN model test results for KVLCC2.

Comparisons of turning circle advance and tactical diameters compared to the model test results are displayed in Table 4.11. Predicted advance and tactical diameters differ by 2% and 5%, which is considered acceptable because of the margin of the IMO standard limits (which are also displayed in this table). The results are also closer to the model tests than a similar study conducted for the KVLCC2 (He et al. 2022).

Table 4.11: KVLCC2 Predicted turning circle advance (A) and tactical diameter (TD) compared to MARIN model tests and IMO limit.

δ	A (model test) [m]	A (prediction) [m]	A (IMO) [m]	TD (model test) [m]	TD (prediction) [m]	TD (IMO) [m]
35.0	21.59	21.21	31.5	21.72	23.07	35.0
-35.0	22.54	22.1	31.5	23.55	24.29	35.0

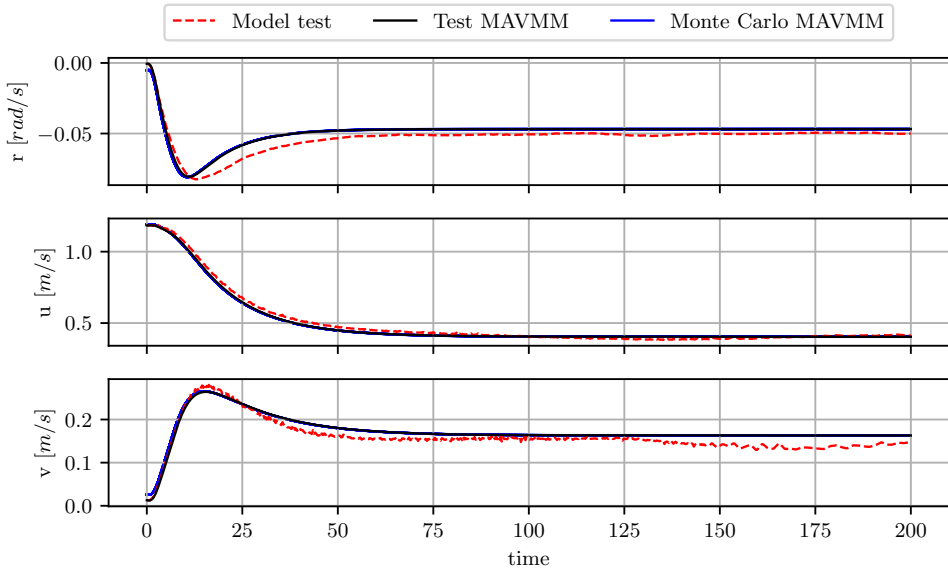


Figure 4.22: Comparison between the predicted turning circle test with MAVMM trained on HSVA data and MARIN model test results for KVLCC2.

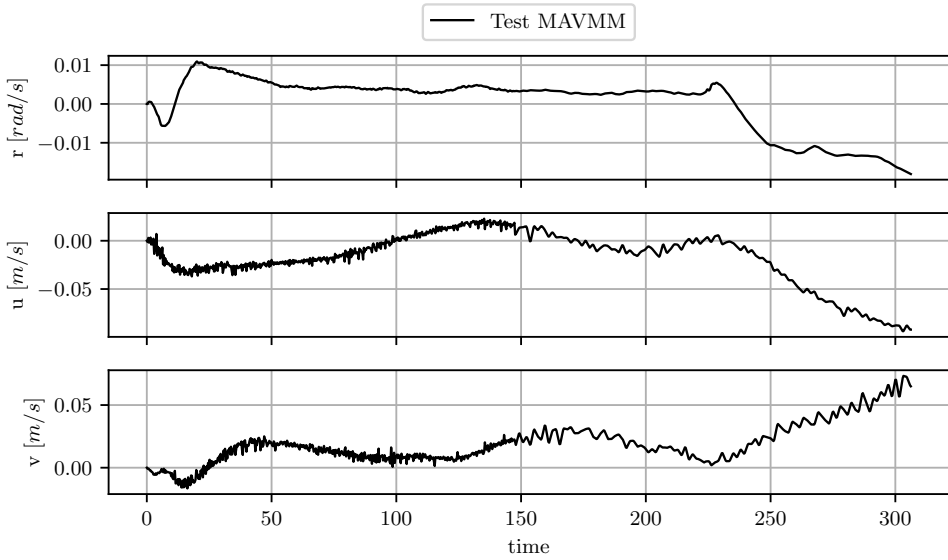


Figure 4.23: The prediction error (prediction minus (-) model test) for the turning circle test with MAVMM trained on HSVA data and MARIN model test results for KVLCC2.

The mean values and standard error (se) of the hydrodynamic derivatives (expressed with prime units for the KVLCC2) obtained with parameter estimation of MAVMM (Eq. (2.17), Eq. (2.18), Eq. (2.19)) applied on all the HSVA data are shown in Table 4.12.

Table 4.12: KVLCC2 MAVMM derivatives (prime units times 1000).

name	mean	se	name	mean	se	name	mean	se
X_{vr}	-11.454	0.272	Y_T	77.34	1.23	N_δ	-1.274	0.003
X_{rr}	-1.406	0.068	Y_r	256.065	0.654	N_r	-105.618	0.179
$X_{\delta\delta}$	-2.719	0.013	Y_v	-24.467	0.02	N_T	-32.523	0.274
X_{uu}	80.508	0.618	Y_{ur}	-252.991	0.658	N_u	0.063	0.001
X_u	-81.415	0.618	Y_u	-0.119	0.003	N_v	-7.156	0.016
						$N_{T\delta}$	-391.596	0.941
						$N_{vv\delta}$	-19.257	0.089
						N_{ur}	102.252	0.183

4.2.3 Inverse dynamics

The capability of the inverse dynamics on simulated data was also investigated in Paper 2. The hydrodynamic derivatives within the manoeuvring model can be identified exactly at ideal conditions for the parameter estimation with no measurement noise and a perfect estimator. For example, artificial data from a turning circle test can be simulated by a predefined/true manoeuvring model. The hydrodynamic derivatives within the manoeuvring model can be identified with the same values. Results from such a simulation are presented in Figure 4.24, where the regression has identified the true values precisely.

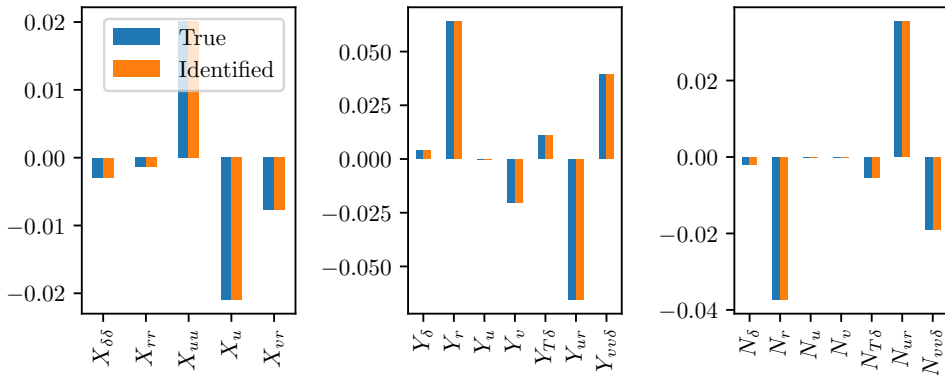


Figure 4.24: True and regressed hydrodynamic derivatives in MAVMM identified with Inverse dynamics and OLS regression on a simulated turning circle with MAVMM.

4.2.4 Preprocessing

The low-pass filter is a prevalent alternative to preprocessing the model test data, as opposed to the EKF used by the proposed parameter estimation. In order to investigate which filter is the most effective, the proposed parameter estimation was run on the wPCC model test data with the EKF + RTS smoother replaced with a low-pass filter. The low-pass filter applies a first-order linear digital Butterworth filter twice (once forward and once backward) for zero-phase conditions (Virtanen et al. 2020). Figure 4.25 displays the average simulation error \overline{RMSE} with low-pass filters at various cutoff frequencies for all wPCC model tests. Corresponding error with parameter estimation using EKF + RTS is also presented in the figure. The simulation error for each model test is expressed as the root mean square error $RMSE$ (Eq. (4.10)) of the distance between the position from the model test and simulation.

$$RMSE = \sqrt{\frac{\sum_{n=1}^N (d_n^2)}{N}} \quad (4.10)$$

where d_n is the euclidean distance for each time step between the model test positions (x_0, y_0) and the predicted positions. The simulations show that high accuracy can be

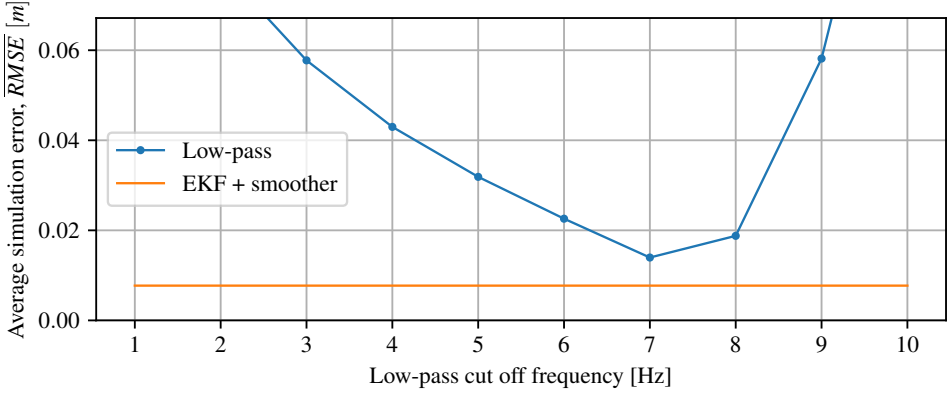


Figure 4.25: Average simulation error with MAVMM fitted on wPCC model test data using low-pass filters with various cutoff frequencies or EKF.

obtained using a low-pass filter as the preprocessor if an optimal cutoff frequency is selected. The low-pass filter's accuracy decreases quickly at lower or higher frequencies. Higher cutoff frequencies result in too much measurement error in the data, which causes the OLS regression to perform poorly. In extreme cases, it is similar to having no filter. An extremely low cutoff frequency removes too much, including parts of the actual signal. The results show that the low-pass filter with a 7 Hz cutoff frequency has the lowest error rate among the low-pass filters. The EKF + RTS method in the parameter estimation has an even lower error rate, which is why it is used as the preprocessor in the proposed parameter estimation.

Conclusions

The main conclusions are presented in this section with respect to the main objective of this thesis:

develop system identification methods for grey box models with good generalization of the model scale rigid body ship dynamics in calm waters.

The conclusions are categorized by the goals that comprise this objective.

Roll model

The first goal of the thesis was to use model test data to develop a model for the calm water rigid body ship dynamics in the roll degree of freedom. Three candidate models were considered:

- the linear roll motion model
- the quadratic roll motion model
- the cubic roll motion model

Data from 250 roll decay tests obtained from SSPA were used to evaluate these models. The linear model was not as accurate as the nonlinear models. The quadratic model was almost as accurate as the cubic model and is expected to have a higher degree of generalization with fewer parameters in the model. Therefore, the quadratic model is the best description for the roll motion.

Predictions with the original Ikeda's method were also conducted for some of the ships that exceeded the limits of the simplified Ikeda's method. These predictions were in much better agreement with the dampings from the model tests. These results indicate that the observed deviations with the simplified Ikeda's method are the result of extrapolation rather than errors inherent to the original Ikeda's method.

A grey-box correction model of the simplified Ikeda's method and a complete black-box model to predict ship roll damping were proposed in Paper 1. The proposed models yield better predictions than the simplified Ikeda's method outside its limits and worse predictions within its limits. Applying corrections to the simplified Ikeda's method outside its limits is therefore not enough for obtaining useful roll damping predictions for modern ships; an additional course of action is necessary. Further research efforts must focus on updating and improving the simplified Ikeda's method.

Manoeuvring model

The second goal of this thesis was to increase the complexity and uncertainty of the modelling by adding the surge, sway, and yaw degrees of freedom. This goal addresses the manoeuvring problem.

It is demonstrated in Paper 2 that the hydrodynamic derivatives within a manoeuvring model can be identified exactly in ideal conditions with no measurement noise and a perfect estimator. Such a result appears during the identification of parameters in a manoeuvring model on data from simulations with the same manoeuvring model. System identification on actual model tests has the challenge of handling the measurement noise and the model uncertainty. A new system identification method has been proposed in Paper 2, where a preprocessor with an EKF and an RTS smoother are run in iteration for a set of candidate manoeuvring models to handle both the measurement noise and model uncertainty. System identification with the proposed pre-processor has higher accuracy than when low-pass filters are applied. Parameter estimation with no filter or a low-pass filter with the wrong settings result in inaccurate estimations.

The linearization in the EKF may threaten stability, which can be a problem for sparse time series with longer time steps. This was not a problem for the present test cases, with very high frequency data (100 Hz). Using the unscented Kalman filter (UKF) instead of the EKF can resolve stability issues. This resolution has not been examined further in this thesis.

Multicollinearity was a significant problem with the AVMM for both the wPCC and KVLCC2 data. Consequently, some of the regressed hydrodynamic derivatives in the AVMM have unphysically large values and substantial uncertainties. The model is still mathematically correct; the regressed polynomials fit the training data well. The regressed polynomial could be the sum of large counteracting coefficients. The model is effective when the states are similar to the training data. When extrapolating, the balance between these massive derivatives may be disturbed, which quickly yields significant extrapolation errors. This behavior occurred for the wPCC test case when predicting forces and moments with the AVMM on unseen validation data; it is a documented problem (ITTC 2008). The MAVMM has fewer hydrodynamic derivatives with lower multicollinearity and minor extrapolation errors. Including propeller thrust in the manoeuvring model made it possible to obtain high accuracy with fewer hydrodynamic derivatives. An additional concern with a high number of parameters in a model is that the standard manoeuvres used in this paper do not follow the aspect of persistence of excitation. As a result, some of the hydrodynamic derivatives might not be identifiable (Revestido Herrero and Velasco González 2012). For instance, the model is exposed to only two rudder angles in the majority of the data during the zigzag tests. A series of step responses used in (Miller 2021) provides a better excitation, but requires a large amount of space. Wider space is possible during lake experiments, but not in a narrow basin. The model generalization therefore must be addressed, as seen in the next section.

Model generalization

The third goal of this thesis was model generalization. In order to be of practical use in an Internet of Ships (IoS) application, the models must be able to make predictions outside the domain covered by the available data. A model development process for manoeuvring models with a high degree of generalization was proposed in Paper 2. The process was executed along with the proposed parameter estimation technique on the wPCC and KVLCC2 test cases. Turning circles were predicted with high accuracy on models trained on zigzag tests. This result indicates that the models have a high degree of generalization because the turning circles have much larger rudder angles, drift angles, and yaw rates compared to the training zigzag tests.

Future work

A long-term objective of this research is to develop system identification methods for rigid body ship dynamics of full scale ships in real sea conditions. The study of these dynamics is an important sub-component of ship digital twins, which can be used to investigate alternative scenarios of the real ship's operation. The system identification methods can be used in advanced autopilots or unmanned surface vessels (USVs). Multiple aspects of the ship's energy consumption originate from its motions. Components of the motions include added resistance in waves or added resistance from the wind and currents. Prediction models for the ship's dynamics can therefore be used to optimize the energy consumption. The investigation of the ship dynamics in a calm-water laboratory environment conducted in this thesis is one step towards the long-term objective. Possible additions to this research will be discussed further in this section.

System identification of model scale rigid body ship dynamics in waves

The calm water assumption used in this thesis reflects a situation that is rare in reality because the sea is never completely calm. The wind, waves, and currents will always influence the movement of real ships. To expand the research beyond the calm water assumption, the development of system identification methods for more realistic conditions is necessary. Entering the seakeeping sub field of ship dynamics introduces new challenges to the system identification compared to the manoeuvring and roll motions, which are studied in this thesis. Seakeeping comprises two more degrees of freedom: heave and pitch. Both of these factors increase the complexity of the models. More importantly, the constant added mass assumption used in this thesis is no longer valid under the influence of wave forces; this means that alternative system identification methods are needed. Wind, waves, and currents all add many uncertainties to the system identification. Conducting system identification of seakeeping model tests data is a way to control these uncertainties. The influence from the waves can be studied in isolation from the wind and currents. The measurement accuracy of the ship and wave motions is also much higher in the laboratory, which makes system identification of model scale rigid body ship dynamics in waves a worthy next step for the research.

System identification of full scale rigid body ship dynamics in wind and current

The calm water assumption used in this thesis may be valid for ships operating on inland waters or sheltered coastal areas. The validity is especially likely if the calm water assumption is expanded to include the influence of the wind and currents. System identification of the ship's rigid body dynamics can be conducted on data from full-scale operation of ships in these conditions. This would also be a necessary next step for the research because it adds the uncertainties from the wind and current in full scale while excluding the influence from the waves.

System identification of full scale rigid body ship dynamics

Given that a satisfactory system identification can be obtained as described by the two steps above, the logical following step would be to combine them in full-scale operation in wind, currents, and waves. To fulfill the requirements of the research project and as a direct, natural continuation of the system identification methods, the data analysis method and established ship dynamic digital twin models can be used to study how ship dynamics can affect a ship's operational performance (fuel consumption and speed loss) in the open sea. This could be another piece of the ship digital twin project. In particular, after establishing the ship digital twin, some online learning and identification methods must be studied and researched to update the digital twin for various applications for ship operation.

References

- Abkowitz, M. A. (1964). “Ship hydrodynamics - steering and manoeuvrability”. en. In: *Hydro- and Aerodynamics Laboratory, Hydrodynamics Section, Lyngby, Denmark, Report No. Hy-5, Lectures*.
- Alexandersson, M. (2022a). *Code for paper system identification of vessel manoeuvring models*. DOI: 10.5281/zenodo.7185580.
- Alexandersson, M. (2022b). *Rolldecay-estimators*. DOI: 10.5281/ZENODO.7299344.
- Alexandersson, M. (2022c). “wpcc manoeuvring model tests”. en. In: 2. DOI: 10.17632/j5zdrhr9bf.2.
- Alexandersson, M., M. Kjellberg, W. Mao, and J. W. Ringsberg (2021a). “Prediction of roll motion using fully nonlinear potential flow and ikeda’s method”. In: *Proceedings of the thirty-first (2021) international ocean and polar engineering conference*. Rhodes, Greece. ISBN: 978-1-880653-82-1.
- Alexandersson, M., W. Mao, and J. W. Ringsberg (2021b). “Analysis of roll damping model scale data”. In: *Ships and Offshore Structures* 16.sup1, pp. 85–92. ISSN: 1744-5302. DOI: 10.1080/17445302.2021.1907070.
- Alexandersson, M., W. Mao, and J. W. Ringsberg (2022a). “System identification of vessel manoeuvring models”. en. In: *Ocean Engineering* 266. ISSN: 0029-8018. DOI: 10.1016/j.oceaneng.2022.112940.
- Alexandersson, M., D. Zhang, W. Mao, and J. W. Ringsberg (2022b). “A comparison of ship manoeuvrability models to approximate ship navigation trajectories”. In: *Ships and Offshore Structures*. ISSN: 1744-5302. DOI: 10.1080/17445302.2022.2067409.
- Araki, M., H. Sadat-Hosseini, Y. Sanada, K. Tanimoto, N. Umeda, and F. Stern (2012). “Estimating maneuvering coefficients using system identification methods with experimental, system-based, and cfd free-running trial data”. en. In: *Ocean Engineering* 51, pp. 63–84. ISSN: 0029-8018. DOI: 10.1016/j.oceaneng.2012.05.001.
- Aslam, S., M. P. Michaelides, and H. Herodotou (2020). “Internet of ships: A Survey on Architectures, Emerging Applications, and Challenges”. en. In: *IEEE Internet of Things Journal* 7.10, pp. 9714–9727. ISSN: 2327-4662, 2372-2541. DOI: 10.1109/JIOT.2020.2993411.
- Assani, N., P. Matic, and M. Katalinić (2022). “Ship’s digital twin—a review of modelling challenges and applications”. In: *Applied Sciences* 12, p. 6039. DOI: 10.3390/app12126039.
- Åström, K. J. and C. G. Källström (1976). “Identification of ship steering dynamics”. en. In: *Automatica* 12.1, pp. 9–22. ISSN: 0005-1098. DOI: 10.1016/0005-1098(76)90064-9.
- Bollen, K., J. T. Cacioppo, R. M. Kaplan, J. A. Krosnick, and J. L. Olds (2015). *Social, behavioral, and economic sciences perspectives on robust and reliable science*. en. Report of the Subcommittee on Replicability in Science Advisory Committee to the National Science Foundation Directorate for Social, Behavioral, and Economic Sciences. National Science Foundation, p. 21. URL: https://www.nsf.gov/sbe/AC_Materials/SBE_Robust_and_Reliable_Research_Report.pdf.
- Brix, J. E. (1993). *Manoeuvring technical manual*. isbn: 978-3-87743-902-9. en. Seehafen-Verlag. ISBN: 978-3-87743-902-9.

- Brown, R. G. and P. Y. C. Hwang (1997). *Introduction to random signals and applied kalman filtering : with matlab exercises and solutions*. Wiley. ISBN: 978-0-471-12839-7.
- Chen, B.-Q., C. Guedes Soares, and P. Videiro (2021). *Review of digital twin of ships and offshore structures*. CRC Press. ISBN: 978-1-00-321658-2. DOI: 10.1201/9781003216582-50.
- Fossen, T. I. (2021). *Handbook of marine craft hydrodynamics and motion control*. English. 2nd edition. Hoboken, NJ: Wiley. ISBN: 978-1-119-57505-4.
- France, W. N., M. Levadou, T. W. Treakle, J. R. Paulling, R. K. Michel, and C. Moore (2001). “An investigation of head-sea parametric rolling and its influence on container lashing systems”. en. In: *SNAME Annual Meeting 2001 Presentation*, p. 24.
- Froude, W. (1861). “On the rolling of ships”. In: *Transactions of the Institution of Naval Architects* vol. 2, pp. 180–227.
- Galeazzi, R., M. Blanke, and N. K. Poulsen (2013). “Early detection of parametric roll resonance on container ships”. In: *IEEE Transactions on Control Systems Technology* 21.2, pp. 489–503. ISSN: 1063-6536, 1558-0865. DOI: 10.1109/TCST.2012.2189399.
- He, H.-W., Z.-H. Wang, Z.-J. Zou, and Y. Liu (2022). “Nonparametric modeling of ship maneuvering motion based on self-designed fully connected neural network”. en. In: *Ocean Engineering* 251, p. 111113. ISSN: 00298018. DOI: 10.1016/j.oceaneng.2022.111113.
- Himeno, Y. (1981). “Prediction of ship roll damping - state of the art.” In: *University of Michigan Department of Naval Architecture and Marine Engineering, (Report)* 239. URL: <http://resolver.tudelft.nl/uuid:2d4991a4-96ac-4935-b2a3-e712effd744d>.
- Ikeda, Y. (1979). “Velocity field around ship hull in roll motion”. en. In: *University of Osaka Prefecture, Department of Naval Architecture, Japan, Report No. 00406, Published in: Journal of Society of Naval Architects of Japan, No. 171, 1978*. URL: <https://repository.tudelft.nl/islandora/object/uuid%3Ac20c11e0-0df3-4c76-84bb-0f24ab0e517f> (visited on 05/14/2020).
- IMO (2002). *Standards for ship manoeuvrability, resolution msc 137(76)*. URL: [https://wwwcdn.imo.org/localresources/en/KnowledgeCentre/IndexofIMOResolutions/MSResolutions/MSC.137\(76\).pdf](https://wwwcdn.imo.org/localresources/en/KnowledgeCentre/IndexofIMOResolutions/MSResolutions/MSC.137(76).pdf).
- IMO (2006). *1200 - interim guidelines for alternative assessment of the weather criterion - netherlands regulatory framework (nerf) – maritime*.
- ITTC (2008). *The maneuvering committee of ittc, final report and recommendations to the 25th ittc, in proceedings of the 25th international towing tank conference*. URL: https://ittc.info/media/3461/volume1_6manoeuvringcommittee.pdf.
- Kawahara, Y., K. Maekawa, and Y. Ikeda (2011). “A simple prediction formula of roll damping of conventional cargo ships on the basis of ikeda’s method and its limitation”. en. In: *Contemporary ideas on ship stability and capsizing in waves*. Ed. by M. Almeida Santos Neves, V. L. Belenky, J. O. de Kat, K. Spyrou, and

- N. Umeda. Fluid Mechanics and Its Applications. Dordrecht, pp. 465–486. ISBN: 978-94-007-1482-3. DOI: 10.1007/978-94-007-1482-3_26.
- Lang, X., D. Wu, and W. Mao (2022). “Comparison of supervised machine learning methods to predict ship propulsion power at sea”. en. In: *Ocean Engineering* 245, p. 110387. ISSN: 00298018. DOI: 10.1016/j.oceaneng.2021.110387.
- Leifsson, L. P., H. Sævarsdóttir, S. Þ. Sigurðsson, and A. Vésteinsson (2008). “Grey-box modeling of an ocean vessel for operational optimization”. en. In: *Simulation Modelling Practice and Theory*. EUROSIM 2007 16.8, pp. 923–932. ISSN: 1569-190X. DOI: 10.1016/j.simpat.2008.03.006.
- Lindskog, P. and L. Ljung (1995). “Tools for semiphysical modelling”. en. In: *International Journal of Adaptive Control and Signal Processing* 9.6, pp. 509–523. ISSN: 08906327, 10991115. DOI: 10.1002/acs.4480090605.
- Liu, G., R. Perez, J. A. Muñoz, and F. Regueira (2016). “Internet of ships: The Future Ahead”. en. In: *World Journal of Engineering and Technology* 4.3, pp. 220–227. DOI: 10.4236/wjet.2016.43D027.
- Lorenz, E. N. (1963). “Deterministic nonperiodic flow”. EN. In: *Journal of the Atmospheric Sciences* 20.2, pp. 130–141. ISSN: 0022-4928, 1520-0469. DOI: 10.1175/1520-0469(1963)020<0130:DNF>2.0.CO;2.
- Luo, W., C. Guedes Soares, and Z. Zou (2016). “Parameter identification of ship maneuvering model based on support vector machines and particle swarm optimization”. en. In: *Journal of Offshore Mechanics and Arctic Engineering* 138.3, p. 031101. ISSN: 0892-7219, 1528-896X. DOI: 10.1115/1.4032892.
- Major, P., R. Zghyer, H. Zhang, and H. Hildre (2021). “A framework for rapid virtual prototyping: a case study with the gunnerus research vessel”. In: *Ship Technology Research*, pp. 1–13. DOI: 10.1080/09377255.2021.1903128.
- Matusiak, J. (2021). *Dynamics of a rigid ship - with applications, 3rd edition*. ISBN: 978-952-64-0398-4. URL: <https://aaltodoc.aalto.fi:443/handle/123456789/108000>.
- Miller, A. (2021). “Ship model identification with genetic algorithm tuning”. en. In: *Applied Sciences* 11.12, p. 5504. ISSN: 2076-3417. DOI: 10.3390/app11125504.
- Mosteller, F. and J. W. Tukey (1968). *Handbook of social psychology, vol. 2*. Ed. by G. Lindzey and E. Aronson. Addison-Wesley.
- Nielsen, R. E., D. Papageorgiou, L. Nalpantidis, B. T. Jensen, and M. Blanke (2022). “Machine learning enhancement of manoeuvring prediction for ship digital twin using full-scale recordings”. en. In: *Ocean Engineering* 257, p. 111579. ISSN: 00298018. DOI: 10.1016/j.oceaneng.2022.111579.
- Perera, L. P., P. Oliveira, and C. Guedes Soares (2015). “System identification of non-linear vessel steering”. en. In: *Journal of Offshore Mechanics and Arctic Engineering* 137.3, p. 031302. ISSN: 0892-7219, 1528-896X. DOI: 10.1115/1.4029826.
- Piehl, H. P. (2016). “Ship roll damping analysis”. Doctoral thesis. Germany: University of Duisburg-Essen. URL: https://duepublico2.uni-due.de/servlets/MCRFileNodeServlet/duepublico_derivate_00043372/Piehl_Diss.pdf.
- Pongduang, S., C. Chungchoo, and P. Iamraksa (2020). “Nonparametric identification of nonlinear added mass moment of inertia and damping moment characteristics of

- large-amplitude ship roll motion”. en. In: *Journal of Marine Science and Application* 19.1, pp. 17–27. ISSN: 1993-5048. DOI: 10.1007/s11804-020-00129-3.
- Rauch, H. E., C. T. Striebel, and F. Tung (1965). “Maximum likelihood estimates of linear dynamic systems”. In: *AIAA Journal* 3, pp. 1445–1450. ISSN: 0001-1452. DOI: 10.2514/3.3166.
- Revestido Herrero, E. and F. J. Velasco González (2012). “Two-step identification of non-linear manoeuvring models of marine vessels”. en. In: *Ocean Engineering* 53, pp. 72–82. ISSN: 0029-8018. DOI: 10.1016/j.oceaneng.2012.07.010.
- “Holdout evaluation” (2017). en. In: *Encyclopedia of machine learning and data mining*. Ed. by C. Sammut and G. I. Webb. Boston, MA, pp. 624–624. ISBN: 978-1-4899-7687-1. DOI: 10.1007/978-1-4899-7687-1_369.
- Shi, C., D. Zhao, J. Peng, and C. Shen (2009). “Identification of ship maneuvering model using extended kalman filters”. en. In: *International Journal on Marine Navigation and Safety of Sea Transportation* 3.1, p. 6.
- Söder, C.-J., A. Rosén, and M. Huss (2019a). “Ikeda revisited”. en. In: *Journal of Marine Science and Technology* 24.1, pp. 306–316. ISSN: 1437-8213. DOI: 10.1007/s00773-017-0497-z.
- Söder, C.-J., A. Rosén, S. Werner, M. Huss, and J. Kutenkeuler (2019b). “Assessment of ship roll damping through full scale and model scale experiments and semi-empirical methods”. en. In: *Contemporary ideas on ship stability: risk of capsizing*. Ed. by V. L. Belenky, K. J. Spyrou, F. van Walree, M. Almeida Santos Neves, and N. Umeda. Fluid Mechanics and Its Applications. Cham, pp. 177–190. ISBN: 978-3-030-00516-0. DOI: 10.1007/978-3-030-00516-0_10.
- Stanic, V., M. Hadjina, N. Fafandjel, and T. Matulja (2018). “Toward shipbuilding 4.0—an industry 4.0 changing the face of the shipbuilding industry”. In: *Brodogradnja* 69, pp. 111–128. DOI: 10.21278/brod69307.
- Stern, F., K. Agdraup, S. Y. Kim, A. C. Hochbaum, K. P. Rhee, F. Quadvlieg, P. Perdon, T. Hino, R. Broglia, and J. Gorski (2011). “Experience from simman 2008—the first workshop on verification and validation of ship maneuvering simulation methods”. en. In: *Journal of Ship Research* 55.02, pp. 135–147. ISSN: 0022-4502, 1542-0604. DOI: 10.5957/jsr.2011.55.2.135.
- Virtanen, P., R. Gommers, T. E. Oliphant, M. Haberland, T. Reddy, D. Cournapeau, E. Burovski, P. Peterson, W. Weckesser, J. Bright, S. J. van der Walt, M. Brett, J. Wilson, K. J. Millman, N. Mayorov, A. R. J. Nelson, E. Jones, R. Kern, E. Larson, C. J. Carey, Í. Polat, Y. Feng, E. W. Moore, J. VanderPlas, D. Laxalde, J. Perktold, R. Cimrman, I. Henriksen, E. A. Quintero, C. R. Harris, A. M. Archibald, A. H. Ribeiro, F. Pedregosa, and P. van Mulbregt (2020). “scipy 1.0: fundamental algorithms for scientific computing in Python”. en. In: *Nature Methods* 17.3, pp. 261–272. ISSN: 1548-7105. DOI: 10.1038/s41592-019-0686-2.
- Wang, T., G. Li, B. Wu, V. Æsøy, and H. Zhang (2021). “Parameter identification of ship manoeuvring model under disturbance using support vector machine method”. In: *Ships and Offshore Structures*. DOI: <https://doi.org/10.1080/17445302.2021.1927600>.

- Wang, Z. and Z. Zou (2018). *Quantifying multicollinearity in ship manoeuvring modeling by variance inflation factor*. Madrid: ASME 2018 37th International Conference on Ocean, Offshore and Arctic. DOI: 10.1115/OMAE2018-77121.
- Xue, Y., Y. Liu, G. Xue, and G. Chen (2021). “Identification and prediction of ship maneuvering motion based on a gaussian process with uncertainty propagation”. en. In: *Journal of Marine Science and Engineering* 9.8, p. 804. ISSN: 2077-1312. DOI: 10.3390/jmse9080804.
- Yasukawa, H. and Y. Yoshimura (2015). “Introduction of mmg standard method for ship maneuvering predictions”. en. In: *Journal of Marine Science and Technology* 20.1, pp. 37–52. ISSN: 0948-4280, 1437-8213. DOI: 10.1007/s00773-014-0293-y.
- Zhang, F., Y. Q. Sun, L. Magnusson, R. Buizza, S.-J. Lin, J.-H. Chen, and K. Emanuel (2019). “What is the predictability limit of midlatitude weather?” EN. In: *Journal of the Atmospheric Sciences* 76.4, pp. 1077–1091. ISSN: 0022-4928, 1520-0469. DOI: 10.1175/JAS-D-18-0269.1.
- Zhu, M., A. Hahn, Y. Wen, and A. Bolles (2017). “Parameter identification of ship maneuvering models using recursive least square method based on support vector machines”. en. In: *TransNav, the International Journal on Marine Navigation and Safety of Sea Transportation* 11.1, pp. 23–29. ISSN: 2083-6473. DOI: 10.12716/1001.11.01.01.

Initial estimates

The parameter estimation method requires an initial guessed linear manoeuvring model. Initial models for the two test cases have hydrodynamic derivatives that can be calculated with semiempirical formulas (Eq. (A.1)-Eq. (A.9)) taken from (Brix 1993).

$$N_r = -\frac{\pi T^2 \left(\frac{0.039B}{T} - \frac{0.56B}{L} + 0.25 \right)}{L^2} \quad (\text{A.1})$$

$$N'_r = -\frac{\pi T^2 \left(\frac{0.017BCB}{T} - \frac{0.33B}{L} + 0.0833333333333333 \right)}{L^2} \quad (\text{A.2})$$

$$N_v = -\frac{\pi T^2 \left(0.5 + \frac{2.4T}{L} \right)}{L^2} \quad (\text{A.3})$$

$$N'_v = -\frac{\pi T^2 \left(-\frac{0.04B}{T} + \frac{1.1B}{L} \right)}{L^2} \quad (\text{A.4})$$

$$X'_u = \frac{2.0m}{L^3 \rho \left(\pi \sqrt{\frac{L^3}{volume}} - 14 \right)} \quad (\text{A.5})$$

$$Y_r = -\frac{\pi T^2 \left(-\frac{0.08B}{T} + \frac{2.2B}{L} - 0.5 \right)}{L^2} \quad (\text{A.6})$$

$$Y'_r = -\frac{\pi T^2 \left(-\frac{0.0033B^2}{T^2} + \frac{0.67B}{L} \right)}{L^2} \quad (\text{A.7})$$

$$Y_v = -\frac{\pi T^2 \left(\frac{0.4BCB}{T} + 1 \right)}{L^2} \quad (\text{A.8})$$

$$Y'_v = -\frac{\pi T^2 \left(-\frac{5.1B^2}{L^2} + \frac{0.16BCB}{T} + 1 \right)}{L^2} \quad (\text{A.9})$$

Part II

Appended papers

Analysis of roll damping model scale data

M. Alexandersson et al. (2021b). “Analysis of roll damping model scale data”. In: *Ships and Offshore Structures* 16.sup1, pp. 85–92. ISSN: 1744-5302. DOI: 10.1080/17445302.2021.1907070

System identification of vessel manoeuvring models

M. Alexandersson et al. (2022a). “System identification of vessel manoeuvring models”. en. In: *Ocean Engineering* 266. ISSN: 0029-8018. DOI: 10.1016/j.oceaneng.2022.112940